

Thermalization and transient dynamics in Multi-Channel Kondo systems under the quantum quench: Large- N Schwinger-Keldysh approach

Iksu Jang^{1,*} and Po-Yao Chang^{1,†}

¹*Department of Physics, National Tsing Hua University, Hsinchu 30013, Taiwan*

(Dated: March 7, 2023)

Understanding properties in out-of-equilibrium many-body quantum systems is an essential task in modern physics. While cutting-edge numerical methods have been developed, extracting the universal dynamics of generic many-body quantum systems remains a big challenge. The multi-channel Kondo impurity (MCKI) model, one of the exotic phases of matter that hosts an over-screened Kondo state with non-Fermi liquid properties, provides a platform for theoretically studying the universal properties of quantum dynamics in many-body systems. By using the large- N Schwinger-Keldysh approach, we systematically investigate transient dynamics and long-time thermalization properties in MCKI under a sudden change of the Kondo coupling. First, we observe oscillations of physical observables such as spin-spin correlations, the Kondo order parameter, and the Kondo energy density for the initial state being an over-screened Kondo state. These oscillations can be interpreted as the quantum revival of the entangled state that describes the over-screened Kondo state. On the other hand, for the initial state that is the high-temperature Fermi liquid, there are no oscillations due to the de-phasing mechanism. Second, we find thermalization properties such as the thermalization time and the final effective temperature strongly depend on the initial state and the quench protocol. The equilibration happens when the Kondo coupling is suddenly increasing under certain conditions. When the Kondo coupling constant is reduced, we observe incoherent thermalization between the impurity and the conduction electrons from the non-vanishing difference between the final effective temperatures between the Abrikosov fermion representing the impurity and the composite boson composed by the Abrikosov fermion and conduction electrons. Additionally, the quantum cooling effect, the consideration of the $1/N$ correction to the conduction electrons, and quantum Boltzmann equations are discussed. Our approach sets the groundwork for investigations of more complex many-body systems, and our results reveal several universal properties of quantum dynamics and offer deeper insight into quantum thermalization.

CONTENTS

I. Introduction	2
II. Multi-Channel Kondo Impurity (MCKI) Model	3
III. Schwinger-Keldysh formalism	4
A. Large- N : Saddle point equations	4
B. $U(1)$ symmetry & Ward identity	6
C. Kadanoff-Baym equations	7
1. Sum-rules	9
D. Physical observables	10
1. Spin-spin correlation function	10
2. Kondo order parameter & Kondo energy density	11
IV. Numerical results & Analysis	12
A. Initial States & Quench set-up	12
1. Initial States	12
2. Quantum quench set-up	12
B. Spectral functions	14
1. Effective temperature & Thermalization time	14
2. Feedback effect to the conduction electron by the self-energy correction of order $\frac{1}{N}$	16
C. Spin-spin correlation function: $C_{imp}(\mathcal{T}, t_r)$ and $\chi_{imp}(\mathcal{T}, t_r)$.	17
D. Kondo order parameter & Kondo energy density	19

* jisjhm@gmail.com

† pychang@phys.nthu.edu.tw

V. Quantum Boltzmann equations	21
VI. Conclusion	22
Acknowledgements	23
A. Derivation of the large- N saddle point self-consistent equations using the Feynman diagrams	23
B. Preparation of the Initial state	24
1. Kadanoff-Baym equation in the equilibrium	24
2. Kubo-Martin-Schwinger (KMS) condition	24
3. Analytic form of the Green's functions of the conduction electrons	24
4. Flow chart of programming	25
C. Numerical Details of solving the Kadanoff-Baym equations	26
1. Discrete forms of Kadanoff-Baym equations	26
2. Flow chart of solving the discrete KB equations	27
D. Effective temperature of the conduction electron with $1/N$ -self energy correction	28
E. Sanity check: sum-rules	28
F. Evolutions of $\mathcal{C}_{imp}(\mathcal{T}, t_r)$ and $\chi_{imp}(\mathcal{T}, t_r)$ after the quenching for $T_0 = 10T_K$ and $T_0 = 0.4T_K$ cases with $J_1 = 6, 15$.	29
References	30

I. INTRODUCTION

Multi-channel Kondo impurity (MCKI) model [1] is one of the variants of the original Kondo model [2] which considers the conduction electrons of more than one channel coupled to the impurity spin. Since the MCKI model shows exotic properties such as non-Fermi liquid phase [3–14] and fractionalized excitations [6, 15–17], it has been intensively studied for decades using several theoretical methods. Especially, the two-channel Kondo (2CK) model [18–20], which is a minimal model of the MCKI, has been investigated theoretically and proposed its experimental realizations. [21–23].

As the equilibrium properties of MCKI models have been thoroughly studied in the past few decades, the focus has shifted toward their non-equilibrium dynamics. Studying the non-equilibrium properties of MCKIs can provide insight into extracting universal properties of generic many-body systems far from equilibrium. Especially, the fact that the non-Fermi liquid phase appears in the MCKI models makes it more interesting to study due to its relevance to the quantum chaos [24, 25]. Additionally, the existence of fractionalized excitations in the MCKI model [26] serves as a significant motivation for recent researches on its non-equilibrium properties, specifically in relation to the manipulation of qubit states in quantum computing physics.

To study the non-equilibrium physics in the MCKI models, several theoretical methods have been used. One of them is a time-dependent numerical renormalization group (TDNRG) method [27] which can cover the whole time scales in principle [28, 29]. However, it usually requires substantial computing resources. Other approaches, which are more analytical, include the renormalization group method [30], bosonization with the Emery-Kivelson (EK) mapping [31–34], conformal field theory (CFT) approach [35], and large- N methods using $SU(N)$ MCKI model [36, 37]. Most of these studies mainly focus on the universal properties of the non-equilibrium steady states (NESS), such as non-equilibrium transport through the MCKI, rather than the transient non-equilibrium phenomena. Additionally, a holographic approach [38] using the AdS/CFT conjecture is used to study the quantum quench dynamics in the Kondo model.

In light of the paucity of research on non-equilibrium transient behavior in the MCKI model and recent interests on the non-equilibrium phenomena in Sachdev-Ye-Kitaev (SYK) models [39–54], we investigate thermalization and transient non-equilibrium phenomena in the MCKI model using the $SU(N)$ MCKI model [14] and Schwinger-Keldysh formalism with the large- N method. While the previous studies [36, 37] of non-equilibrium phenomena using the $SU(N)$ MCKI model focus on the properties of NESS with the assumption of equilibration, we study general quantum dynamics under a sudden quench of the Kondo coupling without any assumption of equilibration. Since it is well known that the low energy state of the $SU(N)$ MCKI model is given by the non-Fermi liquid state so-called over-screened Kondo state in equilibrium [14], we explicitly study the thermalization and transient dynamics under the sudden quench of the Kondo coupling with different initial states, including the non-Fermi liquid state, and quench protocol in the MCKI model.

To analyze the thermalization in the MCKI model, we calculate the effective temperatures and thermalization times of the two objects. One is an Abrikosov fermion representing the impurity spin and another one is a composite boson composed of

the Abrikosov fermion and the conduction electron. From this analysis, we observe that the system becomes equilibrated only when the Kondo coupling increases in the quenching process while the system shows a non-equilibrated state when the Kondo coupling is decreased. Depending on whether the initial state is given by the non-Fermi liquid state or Fermi liquid state, the thermalization process also shows different behaviors. We found that our results of thermalization have similarities with that in the mixed SYK model, composed of both SYK_2 and SYK_4 terms, discussed in [53]. We also discuss the feedback effect, from the conduction electron, which might be able to make the system fully thermalized. In addition, we observe the quantum cooling effect in our system when the Kondo coupling constant is increased in the quenching process. The effective temperature of the equilibrated state has a lower temperature and the reason can be attributed to the formation of a stronger over-screened Kondo state which has a lower impurity entropy. This quantum cooling effect is reminiscent of algorithmic cooling [55], which is a technique used in quantum information processing to decrease the entropy of a quantum system.

To investigate the non-equilibrium properties in the transient time scale, we consider the physical quantities including the spin-spin correlation functions, the Kondo order parameter, and the Kondo energy density. From the analysis of the spin-spin correlation functions, we observe that the exponential decay rate does not change under the quenching process when the initial state is given by the over-screened state while it changes when the initial state is given by a high-temperature Fermi liquid state. Besides we find that every physical quantity we consider exhibits oscillatory properties with a universal frequency [56] given by the energy cut-off of the conduction electron for the initial state being the over-screened Kondo state but not for the high-temperature Fermi liquid state. These oscillations can be interpreted as the quantum revival of the entangled state that describes the over-screened Kondo state [57]. The absence of oscillations in the high-temperature Fermi liquid state can be attributed to its de-phasing property. On top of the numerical analysis, we discuss the dependence of the equilibration on the final state of the system phenomenologically using the quantum Boltzmann equations.

This paper is organized as follows: In Sec. II, we introduce the $SU(N)$ MCKI model and discuss the Abrikosov fermion representation of the quantum impurity. In Sec. III, we present details of Schwinger-Keldysh formalism in the MCKI model with large- N treatment. Sum rules and Green's function representations of the physical quantities are also presented. Readers who are familiar with the subject can directly go to the results in Sec. IV. In Sec. IV, we first examine the spectral functions and analyze the final temperatures and the thermalization times for different quench protocols. Secondly, we present the analysis of the non-equilibrium properties of the physical quantities including spin-spin correlation functions, the Kondo order parameter, and the Kondo energy density in the transient time scale. In Sec. V, we discuss the phenomenological description of the thermal equilibration using the quantum Boltzmann approach. Finally, we give a conclusion in Sec. VI.

II. MULTI-CHANNEL KONDO IMPURITY (MCKI) MODEL

The model for the Multi-Channel Kondo Impurity system with a time-dependent Kondo coupling is given as follows [7–9, 14]:

$$H_{MCKI}(t) = \sum_{\mathbf{p}} \sum_{i=1}^K \sum_{\alpha=1}^N \epsilon(\vec{p}) c_{i,\alpha}(p) c_{i,\alpha}^\dagger(p) + J_K(t) \sum_{A=1}^{N^2-1} S^A \sum_{i,\alpha,\beta} c_{i,\alpha}^\dagger(r=0) t_{\alpha\beta}^A c_{i,\beta}(r=0) \quad (1)$$

where K , N are a channel number and a spin number respectively and $J_K(t)$ is time dependent Kondo coupling. S^A is a A -component of the spin of an impurity in $SU(N)$ -representation and t^A is one of generators of the $SU(N)$ group.

Here we use a fundamental representation of the $SU(N)$ group which satisfies the following properties:

$$\text{tr}[t^A t^B] = 2\delta_{AB} \quad (2a)$$

$$\sum_{A=1}^{N^2-1} t_{\alpha\beta}^A t_{\gamma\eta}^A = 2 \left(\delta_{\alpha\eta} \delta_{\beta\gamma} - \frac{1}{N} \delta_{\alpha\beta} \delta_{\gamma\eta} \right) \quad (2b)$$

Following [14], we use a Abrikosov fermion representation to express the impurity spin as follows:

$$S^A = \frac{1}{2} \sum_{\alpha,\beta=1}^N f_\alpha^\dagger t_{\alpha\beta}^A f_\beta, \quad \sum_{\alpha=1}^N f_\alpha^\dagger f_\alpha = Q, \quad (3)$$

where Q is a total number of f -fermions.

Then, H_{MCKI} is re-expressed as follows:

$$\begin{aligned} H_{MCKI}(t) &= \sum_{\mathbf{p}} \sum_{i=1}^K \sum_{\alpha=1}^N \epsilon(p) c_{i,\alpha}^\dagger(p) c_{i,\alpha}(p) + J_K(t) \sum_{i=1}^K \sum_{\alpha,\beta,\gamma,\eta} f_\alpha^\dagger f_\beta c_{i,\gamma}^\dagger c_{i,\eta} \left(\delta_{\alpha\eta} \delta_{\beta\gamma} - \frac{1}{N} \delta_{\alpha\beta} \delta_{\gamma\eta} \right) \\ &= \sum_{\mathbf{p}} \sum_{i=1}^K \sum_{\alpha=1}^N \epsilon(p) c_{i,\alpha}^\dagger(p) c_{i,\alpha}(p) + J_K(t) \sum_{i=1}^K \left(\sum_{\alpha,\beta} f_\alpha^\dagger f_\beta c_{i,\beta}^\dagger c_{i,\alpha} - \frac{Q}{N} \sum_{\gamma} c_{i,\gamma}^\dagger c_{i,\gamma} \right) \end{aligned} \quad (4)$$

where $c_{i,\alpha} = c_{i,\alpha}(r=0)$.

III. SCHWINGER-KELDYSH FORMALISM

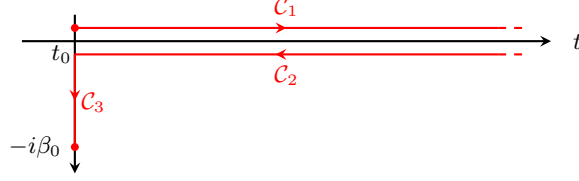


FIG. 1: Keldysh contour $\mathcal{C} = \mathcal{C}_1 \cup \mathcal{C}_2 \cup \mathcal{C}_3$. t_0 is an initial time when an initial state with the temperature $1/\beta_0$ is prepared.

To derive the large- N saddle point equations, we first obtain a path integral formulation of the MCKI Hamiltonian. The resulting partition function and the action are given as follows:

$$Z = \text{tr}[\rho(t)] = \int \mathcal{D}(c^\dagger, c) \int \mathcal{D}(f^\dagger, f) \int \mathcal{D}\lambda e^{iS_{MCKI}}, \quad (5a)$$

$$S_{MCKI} = \int_{\mathcal{C}} dz \left[\sum_{i=1}^K \sum_{\alpha=1}^N \sum_p c_{i,\alpha}^\dagger(p, z) [i\partial_z - \epsilon(p, z)] c_{i\alpha}(p, z) + \sum_{\alpha=1}^N f_\alpha^\dagger(z) [i\partial_z - \lambda(z)] f_\alpha(z) \right. \\ \left. + \lambda(z)Q - J_K(z) \sum_{i=1}^K \sum_{\alpha,\beta=1}^N c_{i,\alpha}^\dagger(z) c_{i,\beta}(z) \left(f_\beta^\dagger(z) f_\alpha(z) - \frac{Q}{N} \delta_{\alpha\beta} \right) \right] \quad (5b)$$

where the Keldysh contour \mathcal{C} is depicted in Fig. 1 and $c_{i,\alpha}(z) = c_{i,\alpha}(r=0, z) = \frac{1}{\sqrt{N_{site}}} \sum_p c_{i,\alpha}(p, z)$ is a conduction electron operator at the impurity site $r=0$. Here Lagrangian multiplier $\lambda(z)$ is introduced to make the Hilbert space of f -electrons restricted for every time indices z .

To construct an effective action defined on the impurity site only, all bulk conduction electrons $c_{i,\alpha}(z, r \neq 0)$ are integrated. The resulting action is given as follows:

$$Z = \int \mathcal{D}(c_{bulk}^\dagger, c_{bulk}) \int \mathcal{D}(c^\dagger(0), c(0)) \int \mathcal{D}(f^\dagger, f) \int \mathcal{D}\lambda e^{iS_{MCKI}} \\ \approx \int \mathcal{D}(c^\dagger(0), c(0)) \int \mathcal{D}(f^\dagger, f) \int \mathcal{D}\lambda e^{iS_{MCKI, r=0}}, \quad (6a)$$

$$S_{MCKI, r=0} = \int_{\mathcal{C}} dz \left[\sum_{i=1}^K \sum_{\alpha=1}^N \int_{\mathcal{C}} dz' c_{i,\alpha}^\dagger(z) G_{c,0}^{-1}(z, z') c_{i,\alpha}(z') + \sum_{\alpha=1}^N f_\alpha^\dagger(z) [i\partial_z - \lambda(z)] f_\alpha(z) \right. \\ \left. + \lambda(z)Q - J_K(z) \sum_{i=1}^K \sum_{\alpha,\beta=1}^N c_{i,\alpha}^\dagger(z) c_{i,\beta}(z) \left(f_\beta^\dagger(z) f_\alpha(z) - \frac{Q}{N} \delta_{\alpha\beta} \right) \right] \quad (6b)$$

where

$$G_{c,0}(z, z') = \frac{1}{N_{site}} \sum_p [i\partial_z - \epsilon(p, z)]_{z,z'}^{-1}, \quad (7)$$

is a free Green's function of conduction electron at the impurity site. Now all degrees of freedom in the $S_{MCKI, r=0}$ are defined on the impurity site only.

A. Large- N : Saddle point equations

Now we will consider the Large- N limit following [14]. With settings

$$K = N\gamma, \quad J_K(z) = \frac{J(z)}{N}, \quad Q = q_0 N, \quad (8)$$

$N \rightarrow \infty$ limit is taken for fixed values of the γ , $J(z)$ and q_0 .

To derive the effective action for the saddle point approximations, we first introduce the new boson field $B_i(z)$ to the action (6b) by using the Hubbard-Stratonovich transformation. Then,

$$\begin{aligned} Z = & \int \mathcal{D}(c^\dagger, c) \int \mathcal{D}(f^\dagger, f) \int \mathcal{D}\lambda e^{iS_{MC KI, r=0}} = \int \mathcal{D}(c^\dagger, c) \int \mathcal{D}(f^\dagger, f) \int \mathcal{D}\lambda \int \mathcal{D}(B^\dagger, B) \\ & \times \exp \left[i \int_{\mathcal{C}} dz \left\{ \sum_{i=1}^K \sum_{\alpha=1}^N \int_{\mathcal{C}} dz' c_{i,\alpha}^\dagger(z) G_c^{-1}(z, z') c_{i,\alpha}(z') + \sum_{\alpha=1}^N \int_{\mathcal{C}} dz' f_\alpha^\dagger(z) G_{f,0}^{-1}(z, z') f_\alpha(z) \right. \right. \\ & + N\lambda(z)q_0 - \frac{1}{J(z)} \sum_{i=1}^K B_i^\dagger(z) B_i(z) - \frac{1}{\sqrt{N}} \sum_{i=1}^K \sum_{\alpha} \left(B_i^\dagger(z) f_\alpha^\dagger(z) c_{i,\alpha}(z) \right. \\ & \left. \left. + B_i(z) c_{i,\alpha}^\dagger(z) f_\alpha(z) \right) \right\} \Bigg] \end{aligned} \quad (9)$$

where

$$G_c^{-1}(z, z') = G_{c,0}^{-1}(z, z') + \frac{q_0 J(z)}{N} \delta_{\mathcal{C}}(z - z') \approx G_{c,0}^{-1}(z, z'), \quad (10a)$$

$$G_{f,0}^{-1}(z, z') = [i\partial_z - \lambda(z)]\delta(z - z'). \quad (10b)$$

Note that the $\frac{1}{N}$ correction to the $G_c^{-1}(z, z')$ is ignored and the $G_{c,0}(z, z')$ (Eq. (7)) is used in the follow-up self-consistent calculations.

Since the action Eq. (9) is quadratic in c^\dagger and c , we can integrate out the c fields. Then,

$$\begin{aligned} Z = & \int \mathcal{D}(f^\dagger, f) \int \mathcal{D}\lambda \int \mathcal{D}(B^\dagger, B) \det \left(-iG_c^{-1}(z, z') \right) \\ & \times \exp \left[i \int_{\mathcal{C}} dz \left\{ \sum_{\alpha=1}^N \int_{\mathcal{C}} dz' f_\alpha^\dagger(z) G_{f,0}^{-1}(z, z') f_\alpha(z') + N\lambda(z)q_0 - \frac{1}{J(z)} \sum_{i=1}^K B_i^\dagger(z) B_i(z) \right. \right. \\ & \left. \left. - \sum_{i=1}^K \sum_{\alpha=1}^N \frac{1}{N} \int_{\mathcal{C}} dz' B_i^\dagger(z) f_\alpha^\dagger(z) G_c(z, z') B_i(z') f_\alpha(z') \right\} \right] \end{aligned} \quad (11)$$

Now let us introduce bi-local fields $Q(z, z')$, $\bar{Q}(z, z')$, $\Sigma_f(z, z')$ and $\Sigma_B(z, z')$ to decouple the interaction vertex in the action (11) by using the following identities:

$$\mathcal{N} \int \mathcal{D}(\Sigma_b^*, \Sigma_b) \int \mathcal{D}Q \exp \left[N \int_{\mathcal{C}} dz \int_{\mathcal{C}} dz' \Sigma_b(z', z) \left(Q(z, z') + \frac{i}{N} \sum_{\alpha=1}^N b_\alpha(z) b_\alpha^\dagger(z') \right) \right] = 1 \quad (12a)$$

$$\mathcal{N}' \int \mathcal{D}(\Sigma_F^*, \Sigma_F) \int \mathcal{D}\bar{Q} \exp \left[K \int_{\mathcal{C}} dz \int_{\mathcal{C}} dz' \Sigma_F(z', z) \left(\bar{Q}(z, z') + \frac{i}{K} \sum_{i=1}^K F_i(z) F_i^\dagger(z') \right) \right] = 1 \quad (12b)$$

where \mathcal{N} and \mathcal{N}' are a normalization constants.

The resulting effective action is given as follows:

$$Z = \int \mathcal{D}\lambda \int \mathcal{D}(\Sigma_f^*, \Sigma_f) \int \mathcal{D}(Q^*, Q) \int \mathcal{D}(\Sigma_B^*, \Sigma_B) \int \mathcal{D}(\bar{Q}^*, \bar{Q}) e^{iS_{eff}[\bar{Q}, Q, \Sigma_f, \Sigma_B, \lambda]}, \quad (13a)$$

$$\begin{aligned} \frac{S_{eff}[\bar{Q}, Q, \Sigma_f, \Sigma_B, \lambda]}{N} = & \int_{\mathcal{C}} dz \int_{\mathcal{C}} dz' \left\{ q_0 \delta(z - z') \lambda(z) - \gamma \bar{Q}(z', z) Q(z', z) G_c(z, z') \right. \\ & \left. - i \Sigma_f(z, z') Q(z', z) - i \gamma \Sigma_B(z, z') \bar{Q}(z', z) \right\} - i \text{tr} \ln [G_{f,0}^{-1}(z, z') - \Sigma_f(z, z')] \\ & + i \gamma \text{tr} \ln [J^{-1}(z) \delta(z - z') - \Sigma_B(z, z')]. \end{aligned} \quad (13b)$$

Since the effective action S_{eff} Eq. (13b) is $\mathcal{O}(N)$ order, the saddle point equations become exact in the $N \rightarrow \infty$ limit. The resulting saddle point equations are given as follows:

$$\Sigma_f(z, z') = i\gamma G_B(z', z)G_c(z, z') \quad (14a)$$

$$\Sigma_B(z, z') = iG_f(z', z)G_c(z, z') \quad (14b)$$

$$G_f(z, z') = [(G_{f,0}^{-1} - \Sigma_f)^{-1}]_{z,z'} \quad (14c)$$

$$G_B(z, z') = [(-J^{-1}(z) + \Sigma_B)^{-1}]_{z,z'} \quad (14d)$$

$$q_0 = -iG_f(z, z + 0^+) \quad (14e)$$

where the fields $Q(z, z')$ and $\bar{Q}(z, z')$ are replaced with $G_f(z, z')$ and $G_B(z, z')$ based on the following definitions of the contour-ordered Keldysh Greens functions:

$$G_f(z, z') = -\frac{i}{N} \sum_{\alpha=1}^N \langle \mathcal{T}_C f_\alpha(z) f_\alpha^\dagger(z') \rangle, \quad (15a)$$

$$G_B(z, z') = -\frac{i}{K} \sum_{i=1}^K \langle \mathcal{T}_C B_i(z) B_i^\dagger(z') \rangle \quad (15b)$$

where \mathcal{T}_C is a contour-ordering operator.

Eqs. (14c) and (14d) can be transformed to the form of the integro-differential equations as follows:

$$(i\partial_z - \lambda(z))G_f(z, z') - \int_C d\bar{z} \Sigma_f(z, \bar{z})G_f(\bar{z}, z') = \delta_C(z - z'), \quad (16a)$$

$$(-i\partial_{z'} - \lambda(z'))G_f(z, z') - \int_C d\bar{z} G_f(z, \bar{z})\Sigma_f(\bar{z}, z') = \delta_C(z - z'), \quad (16b)$$

$$-\frac{1}{J(z)}G_B(z, z') + \int_C d\bar{z} \Sigma_B(z, \bar{z})G_B(\bar{z}, z') = \delta_C(z - z'), \quad (16c)$$

$$-\frac{1}{J(z')}G_B(z, z') + \int_C d\bar{z} G_B(z, \bar{z})\Sigma_B(\bar{z}, z') = \delta_C(z' - z). \quad (16d)$$

These integro-differential equations are used in deriving the Kadanoff-Baym equations below.

One main difference of the Multi-Channel-Kondo model compared to the Sachdev-Ye-Kitaev model is that there is a constraint on the number of f -fermions which is expressed as Eq. (14e). The number of the f -fermions is determined by $\lambda(z)$. In the equilibrium, $\lambda(z)$ is given by the constant value. However, is it still given by the constant value in the non-equilibrium setting? We will see that the value of the $\lambda(z)$ can be fixed to the initial value λ_0 determined from the initial state from the $U(1)$ symmetry. We also derive Ward-identity in the below section.

B. $U(1)$ symmetry & Ward identity

The action Eq. (6b) is invariant under the following $U(1)$ transformation of the impurity fermion f_σ :

$$f_\sigma(z) \rightarrow e^{i\alpha} f_\sigma(z), \quad f_\sigma^\dagger(z) \rightarrow f_\sigma^\dagger(z) e^{-i\alpha} \quad (17)$$

where α is constant.

From the Noether theorem, $Q = \sum_{\alpha=1}^N f_\alpha^\dagger f_\alpha$ is conserved classically. To derive the quantum version of the Noether theorem and Ward identity, let us consider the local $U(1)$ transformation by considering the non-constant $\alpha(z)$. Under the local $U(1)$ transformation, the action Eq. (6b) transforms as follows

$$S_{MCKI, r=0} \rightarrow S_{MCKI, r=0} - \sum_{\sigma} \int_C dz f_\sigma^\dagger(z) \partial_z \alpha(z) f_\sigma(z) \quad (18)$$

while the Jacobian of the integral measure $\mathcal{D}(f^\dagger, f)$ remains invariant. From the fact that the partition function Z is invariant under the above changes, we can derive the following identity:

$$\begin{aligned} Z &= \int \mathcal{D}(f^\dagger, f) \mathcal{D}(\dots) e^{iS} \rightarrow \int \mathcal{D}(f^\dagger, f) \mathcal{D}(\dots) e^{iS} \left(1 - i \int_C dz f_\sigma^\dagger(z) \partial_z \alpha(z) f_\sigma(z) \right) \\ &\Rightarrow \partial_z \sum_{\sigma} \langle f_\sigma^\dagger(z) f_\sigma(z) \rangle = 0 \end{aligned} \quad (19)$$

which is nothing but a quantum version of the Noether theorem.

Not only the partition function Z but also expectation values of the correlation functions should be invariant under the local $U(1)$ transformation. Considering the two-point correlation function $\langle f_\alpha(z_1) f_\alpha^\dagger(z_2) \rangle$, we can derive the following identity:

$$\begin{aligned} \langle f_\sigma(z_1) f_\sigma^\dagger(z_2) \rangle &= \frac{1}{Z} \int \mathcal{D}(f^\dagger, f) \mathcal{D}(\dots) e^{iS} f_\sigma(z_1) f_\sigma^\dagger(z_2) \\ &\rightarrow \langle f_\sigma(z_1) f_\sigma^\dagger(z_2) \rangle + i \left([\alpha(z_1) - \alpha(z_2)] \langle f_\sigma(z_1) f_\sigma^\dagger(z_2) \rangle - \sum_{\sigma'} \int_C dz \partial_z \alpha(z) \langle f_{\sigma'}^\dagger(z) f_{\sigma'}(z) f_\sigma(z_1) f_\sigma(z_2) \rangle_c \right) \\ &\Rightarrow \partial_z \left(G_f(z_1, z) G_f(z, z_2) \right) = i \left(\delta(z - z_1) - \delta(z - z_2) \right) G_f(z_1, z_2) \end{aligned} \quad (20)$$

which is Ward identity.

In addition to the above identities, we can check that the change of the $\lambda(z)$ on the real axis of the contour \mathcal{C} ($\mathcal{C}_1 \cup \mathcal{C}_2$ in Fig. 1) does not affect to the value of physical quantities using the local $U(1)$ transformation. To see that, suppose an arbitrary physical observable operator $\mathcal{O}(z_1, z_2, \dots)$ which is a composite operator consisting of the impurity spin operator \vec{S} and the conduction electron operator c, c^\dagger . These physical observables are invariant under the local $U(1)$ transformation of the f fermions since the impurity spin operator \vec{S} is invariant under the transformation. Now let us consider the expectation value of the physical observable $\mathcal{O}(z_1, z_2, \dots)$:

$$\begin{aligned} \langle \mathcal{O}(z_1, z_2, \dots) \rangle_{\lambda_0} &= \frac{1}{Z} \int \mathcal{D}(f^\dagger, f) \mathcal{D}(\dots) e^{iS} \mathcal{O}(z_1, z_2, \dots) \\ &\rightarrow \frac{1}{Z} \int \mathcal{D}(f^\dagger, f) e^{iS - i \sum_\sigma \int_C dz (\partial_z) f_\sigma^\dagger(z) f_\sigma(z)} \mathcal{O}(z_1, z_2, \dots) \\ &= \langle \mathcal{O}(z_1, z_2, \dots) \rangle_{\lambda_0 + \partial_z \alpha(z)} \end{aligned} \quad (21)$$

where λ_0 is a constant value of the $\lambda(z)$ on the imaginary axis of the contour \mathcal{C} (\mathcal{C}_3 in Fig. 1). The value of the λ_0 is determined by the initial state.

From the relation Eq. (21), we can see that the change of the $\lambda(z)$ on the real axis of the contour \mathcal{C} ($\mathcal{C}_1 \cup \mathcal{C}_2$) does not affect to the physical quantities. As a result, the value of $\lambda(z)$ can be fixed to λ_0 which is determined from the initial state. In the remaining text, we consider $\lambda(z)$ is given by the constant value λ_0 .

C. Kadanoff-Baym equations

Following the [58], we find Kadanoff-Baym equations in terms of the greater, lesser, retarded, advanced, and Keldysh Green's functions from the Eqs. (14) and (16). The greater, lesser, retarded, advanced, and Keldysh Greens functions are defined as follows:

$$G^>(t, t') = G^{21}(t, t'), \quad G^<(t, t') = G^{12}(t, t'), \quad (22a)$$

$$G^R(t, t') = \frac{1}{2} \left(G^{11}(t, t') - G^{12}(t, t') + G^{21}(t, t') - G^{22}(t, t') \right), \quad (22b)$$

$$G^A(t, t') = \frac{1}{2} \left(G^{11}(t, t') + G^{12}(t, t') - G^{21}(t, t') - G^{22}(t, t') \right), \quad (22c)$$

$$G^K(t, t') = \frac{1}{2} \left(G^{11}(t, t') + G^{12}(t, t') + G^{21}(t, t') + G^{22}(t, t') \right) \quad (22d)$$

where $G^{ij}(t, t') = G(z, z') \Big|_{z \in \mathcal{C}_i, z' \in \mathcal{C}_j}$.

It is well known that the retarded, advanced, and Keldysh Green's functions can be re-expressed in terms of the greater and lesser Greens functions:

$$G^R(t, t') = \Theta(t - t') \left(G^>(t, t') - G^<(t, t') \right), \quad (23a)$$

$$G^A(t, t') = \Theta(t' - t) \left(G^<(t, t') - G^>(t, t') \right), \quad (23b)$$

$$G^K(t, t') = \left(G^<(t, t') + G^>(t, t') \right) \quad (23c)$$

where $\Theta(t)$ is a step function with a value 1/2 at $t = 0$. The expressions for the retarded and advanced Greens functions are nothing but the conventional definitions of the retarded and advanced Greens functions.

However the relations Eq. (23) are not applicable to G_B and $\Sigma_f(\propto G_B)$ since the value of $G_B(z, z')$ has a singularity at $z = z'$ reflected in the differential equation Eq. (16d) while usual Green's functions of fermion and boson fields have a singular derivative at $z = z'$. Related to this fact, the fields B_i and B_i^\dagger also do not follow the usual boson commutation relation which is reflected in the absence of the term $B_i^\dagger(z)\partial_z B_i(z)$ in the action (9). As a result, it is difficult to figure out the properties of the field B in the operator language. It causes a problem or confusion in using the relation Eq. (23) and finding a sum-rule for the G_B . To remedy this problem, it is necessary to find a relation between the G_B and fermion operators f and c . To do that, we introduce a source field $\eta_i(z)$ which couples to the boson field $B_i(z)$ in the partition function Eq. (9) as follows:

$$\begin{aligned} Z[\eta^\dagger, \eta] &= \int \mathcal{D}(c^\dagger, c) \int \mathcal{D}(f^\dagger, f) \int \mathcal{D}\lambda \int \mathcal{D}(B^\dagger, B) \\ &\times \exp \left[i \int_{\mathcal{C}} dz \left\{ \sum_{i=1}^K \sum_{\alpha=1}^N \int_{\mathcal{C}} dz' c_{i,\alpha}^\dagger(z) G_c^{-1}(z, z') c_{i,\alpha}(z') + \sum_{\alpha=1}^N \int_{\mathcal{C}} dz' f_\alpha^\dagger(z) G_{f,0}^{-1}(z, z') f_\alpha(z) \right. \right. \\ &+ N\lambda(z)q_0 - \frac{1}{J(z)} \sum_{i=1}^K B_i^\dagger(z) B_i(z) - \frac{1}{\sqrt{N}} \sum_{i=1}^K \sum_{\alpha} \left(B_i^\dagger(z) f_\alpha^\dagger(z) c_{i,\alpha}(z) \right. \\ &\left. \left. + B_i(z) c_{i,\alpha}^\dagger(z) f_\alpha(z) \right) + \sum_i \left(\eta_i(z) B_i^\dagger(z) + B_i(z) \eta_i^\dagger(z) \right) \right\} \Bigg] \end{aligned} \quad (24)$$

By calculating the $\frac{1}{Z[\eta^\dagger, \eta]} \frac{\delta^2 Z[\eta^\dagger, \eta]}{\delta \eta_i^\dagger(z') \delta \eta_i(z)} \Big|_{\eta^\dagger = \eta = 0}$, we can easily find a following relation:

$$G_B(z, z') = -J(z)\delta_{\mathcal{C}}(z - z') + J(z)J(z')G_\phi(z, z') \quad (25)$$

where a new boson field ϕ and a Green's function are defined as follows:

$$\phi_i(z) = \frac{1}{\sqrt{N}} \sum_{\alpha=1}^N f_\alpha^\dagger(z) c_{i,\alpha}(z), \quad \phi_i^\dagger(z) = \frac{1}{\sqrt{N}} \sum_{\alpha=1}^N c_{i,\alpha}^\dagger(z) f_\alpha(z), \quad (26a)$$

$$G_\phi(z, z') = -\frac{i}{K} \sum_{i=1}^K \langle \mathcal{T}_{\mathcal{C}} \phi_i(z) \phi_i^\dagger(z') \rangle. \quad (26b)$$

Eq. (25) shows the singularity at $z = z'$ of the $G_B(z, z')$ explicitly. By using $G_\phi(z, z')$ instead of the $G_B(z, z')$, we can avoid the singularity issue and Eq. (23) is applicable to the $G_\phi(z, z')$. Additionally, we can easily find a sum-rule for the boson field ϕ , discussed in the next section, from the Eq. (26a).

Using the Eq. (25), the self-consistent saddle point equations(Eqs. (14), (16)) can be re-expressed in terms of the $G_\phi(z, z')$ as follows:

$$\tilde{\Sigma}_f(z, z') = i\gamma J(z)J(z')G_\phi(z', z)G_c(z, z'), \quad (27a)$$

$$\Sigma_B(z, z') = iG_f(z', z)G_c(z, z'), \quad (27b)$$

$$q_0 = -iG_f(z, z+0^+) = -iG_f^<(z, z), \quad (27c)$$

$$[i\partial_z - \lambda_0 + i\gamma J(z)G_c(z, z)]G_f(z, z') - \int_{\mathcal{C}} d\bar{z} \tilde{\Sigma}_f(z, \bar{z})G_f(\bar{z}, z') = \delta_{\mathcal{C}}(z - z'), \quad (27d)$$

$$[-i\partial_{z'} - \lambda_0 + i\gamma J(z')G_c(z', z')]G_f(z, z') - \int_{\mathcal{C}} d\bar{z} G_f(z, \bar{z})\tilde{\Sigma}_f(\bar{z}, z') = \delta_{\mathcal{C}}(z - z'), \quad (27e)$$

$$G_\phi(z, z') + \Sigma_B(z, z') = \int_{\mathcal{C}} d\bar{z} \Sigma_B(z, \bar{z})J(\bar{z})G_\phi(\bar{z}, z') \quad (27f)$$

$$G_\phi(z, z') + \Sigma_B(z, z') = \int_{\mathcal{C}} d\bar{z} G_\phi(z, \bar{z})J(\bar{z})\Sigma_B(\bar{z}, z') \quad (27g)$$

where the relation

$$\Sigma_f(z, z') = -i\gamma J(z)G_c(z, z')\delta_{\mathcal{C}}(z - z') + \tilde{\Sigma}_f(z, z') \quad (28)$$

has been used and $\lambda(z)$ is set to be the constant value λ_0 .

Now let us re-write the above Eqs. (27) in terms of the greater, lesser, retarded, and advanced Green's functions using Eqs. (22) and (23). Then the resulting Kadanoff-Baym equations are given by

$$\left[i\partial_t + i\gamma J(t)G_c^<(t, t) - \lambda_0 \right] G_f^R(t, t') - \int d\bar{t} \tilde{\Sigma}_f^R(t, \bar{t}) G_f^R(\bar{t}, t') = \delta(t - t'), \quad (29a)$$

$$\left[-i\partial_{t'} + i\gamma J(t')G_c^<(t', t') - \lambda_0 \right] G_f^R(t, t') - \int d\bar{t} G_f^R(t, \bar{t}) \tilde{\Sigma}_f^R(\bar{t}, t') = \delta(t - t'), \quad (29b)$$

$$\left[i\partial_t - \lambda_0 + i\gamma J(t)G_c^<(t, t) \right] G_f^>(t, t') - \int d\bar{t} \left[\tilde{\Sigma}_f^>(t, \bar{t}) G_f^A(\bar{t}, t') + \tilde{\Sigma}_f^R(t, \bar{t}) G_f^>(\bar{t}, t') \right] = 0, \quad (29c)$$

$$\left[i\partial_t - \lambda_0 + i\gamma J(t)G_c^<(t, t) \right] G_f^<(t, t') - \int d\bar{t} \left[\tilde{\Sigma}_f^<(t, \bar{t}) G_f^A(\bar{t}, t') + \tilde{\Sigma}_f^R(t, \bar{t}) G_f^<(\bar{t}, t') \right] = 0, \quad (29d)$$

$$G_\phi^R(t, t') + \Sigma_B^R(t, t') = \int d\bar{t} \Sigma_B^R(t, \bar{t}) J(\bar{t}) G_\phi^R(\bar{t}, t'), \quad (29e)$$

$$G_\phi^>(t, t') + \Sigma_B^>(t, t') = \int d\bar{t} \left[\Sigma_B^>(t, \bar{t}) J(\bar{t}) G_\phi^A(\bar{t}, t') + \Sigma_B^R(t, \bar{t}) J(\bar{t}) G_\phi^>(\bar{t}, t') \right], \quad (29f)$$

$$G_\phi^<(t, t') + \Sigma_B^<(t, t') = \int d\bar{t} \left[\Sigma_B^<(t, \bar{t}) J(\bar{t}) G_\phi^A(\bar{t}, t') + \Sigma_B^R(t, \bar{t}) J(\bar{t}) G_\phi^<(\bar{t}, t') \right] \quad (29g)$$

where

$$\tilde{\Sigma}_f^{>/<}(t, t') = i\gamma J(t)J(t')G_\phi^{</>}(t', t)G_c^{>/<}(t, t'), \quad (30a)$$

$$\Sigma_B^{>/<}(t, t') = iG_f^{</>}(t', t)G_c^{>/<}(t, t'), \quad (30b)$$

$$G_f^<(t, t) = iq_0, \quad G_f^>(t, t) = -i(1 - q_0). \quad (30c)$$

Additionally, following identities can be obtained from the definitions of the Green's functions.

$$[G_{c/f/\phi}^{>/<}(t, t')]^* = -G_{c/f/\phi}^{>/<}(t', t), \quad [G_{c/f/\phi}^R(t, t')]^* = G_{c/f/\phi}^A(t', t) \quad (31a)$$

$$[\tilde{\Sigma}_f^{>/<}(t, t')]^* = -\tilde{\Sigma}_f^{>/<}(t', t), \quad [\tilde{\Sigma}_f^R(t, t')]^* = \tilde{\Sigma}_f^A(t', t), \quad (31b)$$

$$[\Sigma_B^{>/<}(t, t')]^* = -\Sigma_B^{>/<}(t', t), \quad [\Sigma_B^R(t, t')]^* = \Sigma_B^A(t', t) \quad (31c)$$

1. Sum-rules

Here we obtain some useful sum-rules which serve as good tools to check numerical results. In expressing the sum-rules, we use the Greens functions in terms of total time $\mathcal{T} = \frac{t+t'}{2}$ and relative time $t_r = t - t'$ shown in the Fig. 5 instead of the t and t' .

For the f -fermions, we can obtain the following trivial sum-rules from the Eq. (30c) and the commutation relation of f fermion $\{f_i, f_i^\dagger\} = 1$:

$$\int \frac{d\omega_r}{2\pi} G_f^<(\mathcal{T}, \omega_r) = iq_0, \quad \int \frac{d\omega_r}{2\pi} G_f^>(\mathcal{T}, \omega_r) = -i(1 - q_0), \quad \int \frac{d\omega_r}{2\pi} A_f(\mathcal{T}, \omega_r) = 1 \quad (32)$$

where

$$G_f^{</>/R}(\mathcal{T}, \omega_r) = \int dt_r e^{-i\omega_r t_r} G_f^{</>/R}(\mathcal{T}, t_r), \quad A_f(\mathcal{T}, t_r) = -2ImG_f^R(\mathcal{T}, t_r). \quad (33)$$

Now let us consider the sum-rule for the ϕ -boson. The sum-rule for the boson ϕ is subtle compared to the f fermion. Using

Eq. (26a), we obtain the following sum-rule for the spectral function of the boson ϕ :

$$\begin{aligned}
\int \frac{d\omega_r}{2\pi} A_\phi(\mathcal{T}, \omega_r) &= \frac{1}{K} \sum_{i=1}^K \langle [\phi_i, \phi_i^\dagger] \rangle = \frac{1}{NK} \sum_{i=1}^K \sum_{\alpha, \beta=1}^N \langle [f_\alpha^\dagger c_{i,\alpha}, c_{i,\beta}^\dagger f_\beta] \rangle \\
&= \frac{1}{NK} \sum_{i=1}^K \sum_{\alpha=1}^N \langle [f_\alpha^\dagger f_\alpha \{c_{i,\alpha}, c_{i,\alpha}^\dagger\} - c_{i,\alpha}^\dagger c_{i,\alpha}] \rangle \\
&= \frac{1}{NK} \sum_{i=1}^K \sum_{\alpha=1}^N [\langle f_\alpha^\dagger f_\alpha \rangle \left(\int \frac{d\omega_r}{2\pi} A_c(\omega) \right) - \langle c_{i,\alpha}^\dagger c_{i,\alpha} \rangle] \\
&= q_0 \int \frac{d\omega}{2\pi} A_c(\omega) + iG_c^<(t=0) = q_0 \nu_c + iG_c^<(t=0)
\end{aligned} \tag{34}$$

where $A_\phi(\mathcal{T}, \omega_r) = \int dt_r e^{-i\omega_r t_r} A_\phi(\mathcal{T}, t_r)$, $A_\phi(\mathcal{T}, t_r) = -2ImG_\phi^R(\mathcal{T}, t_r)$ and ν_c is the filling of the conduction electron defined in the Appendix. B 3.

Lastly, combining the Ward identity Eq. (20) with the Eqs. (27d) and (27e) gives the following relation:

$$\int_{\mathcal{C}} d\bar{z} \left[G_f(z_1, \bar{z}) \tilde{\Sigma}_f(\bar{z}, z) G_f(z, z_2) - G_f(z_1, z) \tilde{\Sigma}_f(z, \bar{z}) G_f(\bar{z}, z_2) \right] = 0. \tag{35}$$

This relation holds for the general values of z , z_1 and z_2 . When $z = z_1 = z_2$, Eq. (35) is reduced to a following relation:

$$\begin{aligned}
&\partial_t G_f^<(t, t') \Big|_{t'=t} + \partial_{t'} G_f^<(t, t') \Big|_{t'=t} \\
&= \int d\bar{t} \left[\tilde{\Sigma}_f^<(t, \bar{t}) G_f^A(\bar{t}, t) + \tilde{\Sigma}_f^R(t, \bar{t}) G_f^<(\bar{t}, t) \right. \\
&\quad \left. - G_f^R(t, \bar{t}) \tilde{\Sigma}_f^<(\bar{t}, t) - G_f^<(t, \bar{t}) \tilde{\Sigma}_f^A(\bar{t}, t) \right] = 0
\end{aligned} \tag{36}$$

which can be also obtained from the Kadanoff-Baym Eq. (29c), (29d) and the fact that $G_f^<(t, t) = iq_0$.

Note that these sum-rules hold for the general non-equilibrium setting. We have used these sum-rules to check the results of the numerical simulations.

D. Physical observables

We derive the expressions of the physical observables in terms of the Greens functions here.

1. Spin-spin correlation function

First, we consider a spin-spin correlation function defined as follows:

$$\Theta(t - t') \frac{\langle \vec{S}_{imp}(t) \cdot \vec{S}_{imp}(t') \rangle}{N^2 - 1} = C_{imp}(t, t') - \frac{i}{2} \chi_{imp}(t, t') \tag{37}$$

where $C_{imp}(t, t')$ and $\chi_{imp}(t, t')$ are a real part of the spin-spin correlation function and spin-susceptibility respectively given by

$$C_{imp}(t, t') = \frac{1}{2} \frac{1}{N^2 - 1} \sum_{A=1}^{N^2-1} \langle \{S_{imp}^A(t), S_{imp}^A(t')\} \rangle, \tag{38a}$$

$$\chi_{imp}(t, t') = i \frac{\Theta(t - t')}{N^2 - 1} \sum_{A=1}^{N^2-1} \langle [S_{imp}^A(t), S_{imp}^A(t')] \rangle. \tag{38b}$$

where A is index of the spin direction.

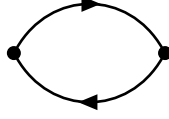


FIG. 2: Feynman diagram of the spin susceptibility $\chi_f(z, z')$ with the order $\mathcal{O}(N^0)$.

To obtain the spin-spin correlation function in terms of the Green's function, we re-express the spin-spin correlation function using the Abrikosov representation (Eq. (3)) and Keldysh formalism as follows:

$$\begin{aligned}
 & \Theta(t - t') \frac{\langle \vec{S}_{imp}(t) \cdot \vec{S}_{imp}(t') \rangle}{N^2 - 1} \\
 &= \frac{\Theta(t - t')}{4(N^2 - 1)} \sum_{A=1}^{N^2-1} \left\langle \mathcal{T}_C f_\alpha^\dagger(z) t_{\alpha\beta}^A f_\beta(z) f_\gamma^\dagger(z') t_{\gamma\eta}^A f_\eta(z') \right\rangle \Big|_{\text{Re}z=t, \text{Re}z'=t'} \\
 &\equiv \Theta(t - t') \mathcal{F}(z, z') \Big|_{\text{Re}z=t, \text{Re}z'=t'}
 \end{aligned} \tag{39}$$

where z and z' are points on Keldysh contour (Fig. 1)

Using the path integral formalism based on the Feynman rules (Eq. (A1)), we calculate value of $\mathcal{F}(z, z')$ of the order $\mathcal{O}(N^0)$ given by Fig. 2. The diagrams with more than one-loop are ignored since they are suppressed in the $N \rightarrow \infty$ limit. The resulting $\mathcal{F}(z, z')$ is given as follows:

$$\mathcal{F}(z, z') = \frac{1}{4} \frac{1}{N^2 - 1} \sum_{A=1}^{N^2-1} t_{\alpha\beta}^A t_{\gamma\eta}^A \left\langle f_\alpha^\dagger(z) f_\beta(z) f_\gamma^\dagger(z') f_\eta(z') \right\rangle = \frac{1}{2} G_f(z, z') G_f(z', z) \tag{40}$$

where Eq. (2) and $\text{tr}[t^A] = 0$ are used.

As a result, the spin-spin correlation function of $\mathcal{O}(N^0)$ order is expressed in terms of the Green's functions as follows:

$$\Theta(t - t') \frac{\langle \vec{S}_{imp}(t) \cdot \vec{S}_{imp}(t') \rangle}{N^2 - 1} = \Theta(t - t') \mathcal{F}(z, z') \Big|_{\text{Re}z=t, \text{Re}z'=t'} = \frac{\Theta(t - t')}{2} G_f^>(t, t') G_f^<(t', t) \tag{41}$$

Then, $C_{imp}(t, t')$ and $\chi_{imp}(t, t')$ are given by

$$C_{imp}(t, t') = \frac{1}{4} \Theta(t - t') [G_f^>(t, t') G_f^<(t', t) + G_f^<(t, t') G_f^>(t', t)], \tag{42a}$$

$$\chi_{imp}(t, t') = i \frac{1}{2} \Theta(t - t') [G_f^>(t, t') G_f^<(t', t) - G_f^<(t, t') G_f^>(t', t)]. \tag{42b}$$

where identities (Eq. (31)) are used.

2. Kondo order parameter & Kondo energy density

In addition to the spin-spin correlation function, we also consider a Kondo order parameter and Kondo energy density defined as follows:

$$\mathcal{O}_{Kondo}(t) = \frac{1}{K} \sum_i \left\langle \vec{S}_{imp}(t) \cdot \vec{s}_{c,i}(t) \right\rangle, \tag{43}$$

$$E_{Kondo}(t) = J_K(t) \sum_{i=1}^K \left\langle \vec{S}_{imp}(t) \cdot \vec{s}_{c,i}(t) \right\rangle = \gamma J(t) \mathcal{O}_{Kondo}(t) \tag{44}$$

where $\vec{s}_{c,i}(t) = \sum_{\alpha, \beta=1}^N c_{i, \alpha}^\dagger(t) t_{\alpha\beta}^A c_{i, \beta}(t)$.

Considering the $J(z)$ field in the partition function $Z(\text{Eq. (6a)})$ as a source field, the $\mathcal{O}_{Kondo}(t)$ is given by

$$\begin{aligned}\mathcal{O}_{Kondo}(t) &= i\gamma \frac{\delta \ln Z[J(z)]}{\delta J(z)} \Big|_{\text{Re}z=t} \\ &= i\gamma \left[\frac{1}{J^2(z)} \sum_{i=1}^K \left\langle B_i^\dagger(z) B_i(z) \right\rangle + \frac{q_0}{N} \sum_{i=1}^K \sum_{\alpha=1}^N \left\langle c_{i,\alpha}^\dagger(z) c_{i,\alpha}(z) \right\rangle \right] \Big|_{\text{Re}z=t} \\ &= iN \left[q_0 G_c^<(t, t) - \frac{1}{J^2(t)} G_B^<(t, t) \right] = iN \left[q_0 G_c^<(t, t) - G_\phi^<(t, t) \right]\end{aligned}\quad (45)$$

where the relation Eq. (25) is used and $\frac{1}{N}$ -correction in the Eq. (10a) is considered. Then,

$$E_{Kondo}(t) = iKJ(t) \left[q_0 G_c^<(t, t) - G_\phi^<(t, t) \right]. \quad (46)$$

IV. NUMERICAL RESULTS & ANALYSIS

To understand the dynamics of the Multi-Channel Kondo system under the quench protocol quantitatively, we have investigated the evolution of several physical quantities such as spectral functions, spin-spin correlation function (Eq. (37)), the Kondo-order parameter (Eq. (45)) and the Kondo energy density (Eq. (46)). Additionally, we have calculated the effective temperature and the thermalization time. To examine how the initial states affect the quench dynamics, we have considered four different initial states with temperatures lower and higher than the Kondo temperature T_K .

A. Initial States & Quench set-up

1. Initial States

Before going to the results of the quench dynamics, we first discuss the properties of the initial states with different given temperatures. To get self-consistent solutions of the initial states with real-time arguments numerically, we followed [39]. For details, see Appendix B.

From the Poor man's RG [59], the Kondo temperature T_K is given by $T_K = \Lambda e^{-\frac{1}{J_0 N_F}}$ where Λ is the energy cut-off and N_F is the density of states near the Fermi energy of the conduction electron given by $\frac{\nu_c}{2\Lambda}$. See Appendix B 3 for details about the conduction electron setting. Based on the Kondo temperature, we have considered five cases with temperatures given by $0.4T_K$, T_K , $1.6T_K$, $5T_K$, and $10T_K$.

For numerical simulations, we used a time lattice of $N_{site} = 8000$ with $\Delta t = 0.1$. Then $\omega_{max} = \frac{\pi}{\Delta t} \approx 31.4$ and $\Delta\omega = \frac{2\omega_{max}}{N_{site}} \approx 0.008$. For settings of conduction electrons, we use $\Lambda = \frac{\omega_{max}}{5} \approx 6.28$ and $\nu_c = 0.5$. The Kondo coupling constant J_0 and the filling of the f -fermion q_0 are set to be 10 and 0.5 respectively. The resulting numerical value of the Kondo temperature is given by around 0.5. In the set-up of numerical values, the energy resolution value $\Delta\omega$ should be the smallest value than any energy scale such as Kondo temperature T_K or temperature T while ω_{max} should be the largest one to get convergent physical solutions. For the γ value, we fix it to be $\gamma = 0.8$. Since it is known that the Multi-Channel Kondo system using the Abrikosov fermion representation with large- N limit shows the over-screened phase for any γ values [14], we expect that there is no qualitative difference in the dynamics depending on the value of γ .

Fig. 3 shows spectral functions of f -fermion and ϕ -boson with different temperatures. As a sanity check, the sum rules in Sec. III C 1 are checked. Note that the Kondo peak develops around the $\omega = 0$ point when the temperature becomes lower than the T_K . The Kondo transition can be seen more clearly in the self energies as shown in Fig. 4.

2. Quantum quench set-up

With the four different initial states, we consider the quantum quench of coupling constant $J(t)$ at $t = 0$ from the initial value J_0 to J_1 . Therefore

$$J(t) = J_0(1 - \Theta(t)) + J_1\Theta(t). \quad (47)$$

For details of the numerical simulation of the Kadanoff-Baym equations, please see Appendix C. In our simulations, the two-dimensional time lattice with the size 600×600 and $\Delta t = 0.1$ is used. Fig. 5 shows a schematic figure for the time lattice used

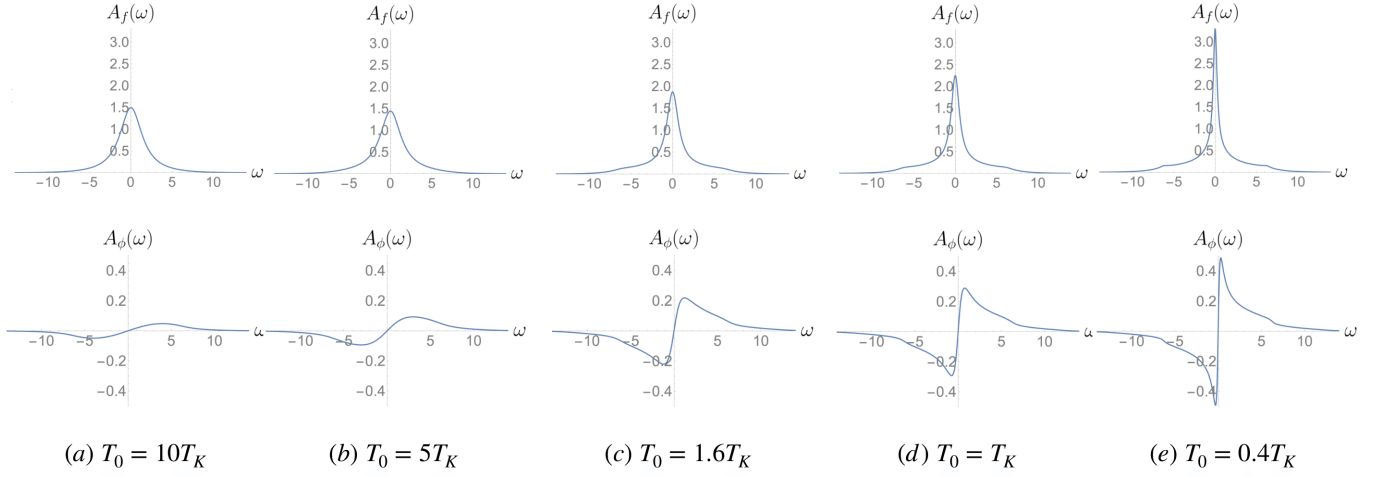


FIG. 3: Spectral functions of f -fermion and ϕ -boson with the temperatures given by $10T_K$, $5T_K$, $1.6T_K$, T_K and $0.4T_K$.

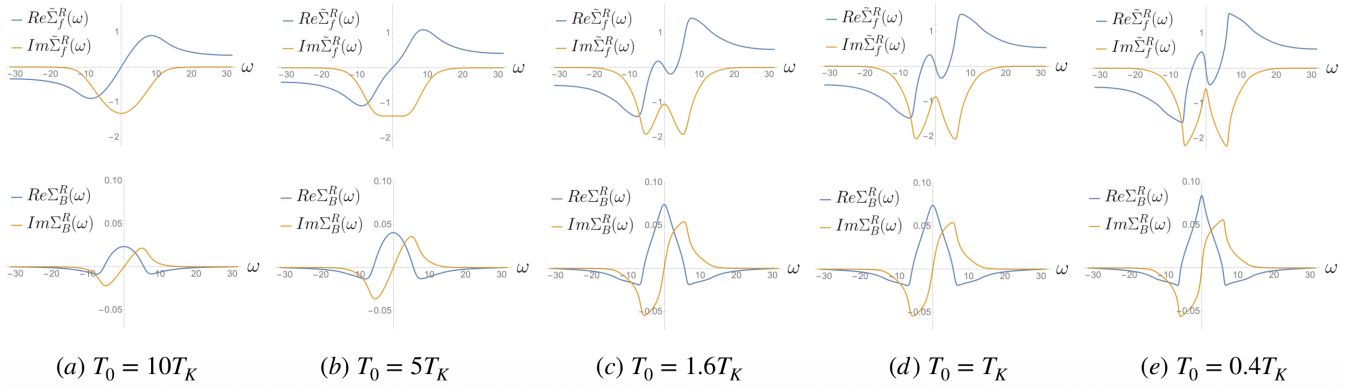


FIG. 4: Self energies of f -fermion and ϕ -boson with the temperatures given by $10T_K$, $5T_K$, $1.6T_K$, T_K and $0.4T_K$.

in the simulations. As numerical values of J_1 , we consider total of nine values given by

$$J_1 = \begin{cases} 6, 7, 8, 9 & < J_0 (= 10) \\ 11, 12, 13, 14, 15 & > J_0 (= 10) \end{cases}. \quad (48)$$

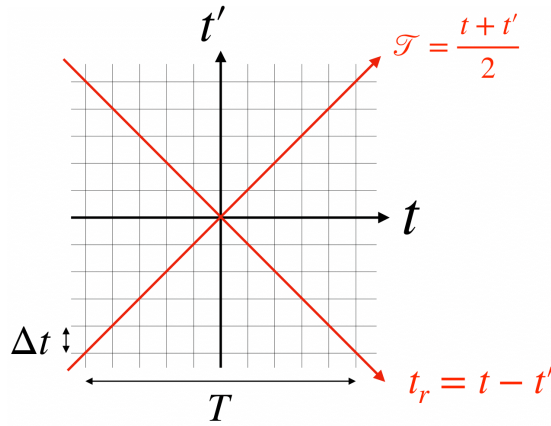


FIG. 5: Two-dimensional time lattice for Kadanoff-Baym solver. \mathcal{T} and t_r are given by $\frac{t+t'}{2}$ and $t - t'$ respectively.

In the analysis, we used transformed coordinates $\mathcal{T} = \frac{t+t'}{2}$ and $t_r = t - t'$ rather than the original coordinates t and t' . In the

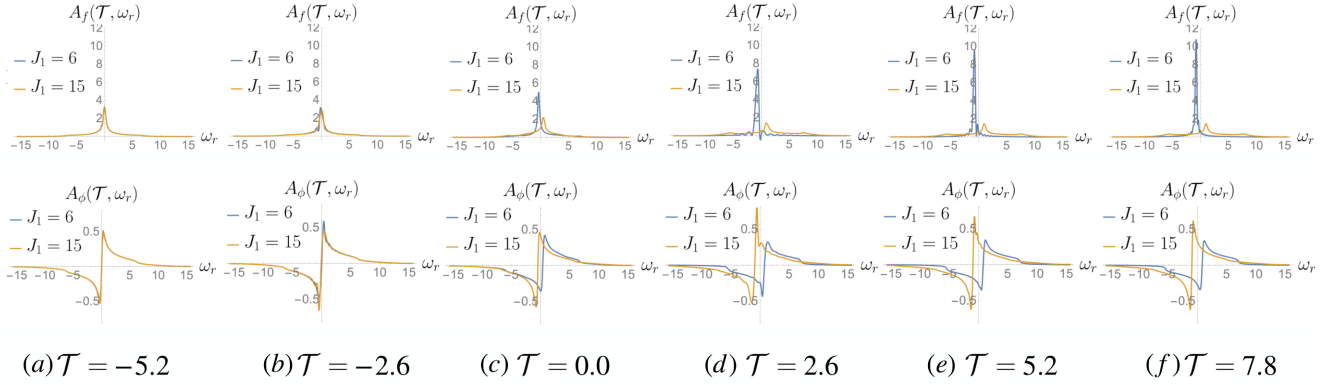


FIG. 6: Evolution of the spectral functions of f -fermion and ϕ -boson for $J_1 = 6$ and $J_1 = 15$ cases with the initial temperature $T_0 = 0.4T_K$.

remaining text, we use Green's functions with the arguments \mathcal{T} and t_r or ω_r where ω_r is a frequency defined in the following Fourier transformation with respect to t_r : $G(\mathcal{T}, \omega_r) = \int dt_r e^{-i\omega_r t_r} G(\mathcal{T}, t_r)$.

B. Spectral functions

As the first quantity to see the effects of the quench, we consider spectral functions. From the spectral functions, we can obtain the effective temperature and the thermalization time under the quench. Since there are not many qualitative differences in the evolutions of the spectral function itself between the cases with different initial temperatures, we show the evolutions of the spectral functions for the initial temperature $T_0 = 0.4T_K$ case with the largest $J_1 (= 15)$ and smallest $J_1 (= 6)$ values in Fig. 6 only. For the numerical result of sum rules as sanity checks, please see Appendix. E.

Since the initial temperature is lower than the Kondo temperature T_K , the spectral function $A_f(\mathcal{T}, \omega_r)$ with $\mathcal{T} = -5.2$ (Fig. 6 (a)) shows a sharp Kondo peak. In $J_1 = 6$ case, the spectral function $A_f(\mathcal{T}, \omega_r)$ shows an oscillating pattern during the evolution. Even when $\mathcal{T} = 7.8$ (Fig. 6 (f)), it still shows a small oscillating near the peak. It is checked that the oscillating pattern disappears at later time around $\mathcal{T} \approx 15$. However, there is no such oscillating pattern appears in the $A_f(\mathcal{T}, \omega_r)$ for $J_1 = 15$ case. In every cases, the center of the $A_f(\mathcal{T}, \omega_r)$ and $A_\phi(\mathcal{T}, \omega_r)$ are moved. This is due to the time-dependent self-energy correction. However the change of the center or chemical potential does not affect the physical observable quantities as discussed in Sec. III B.

1. Effective temperature & Thermalization time

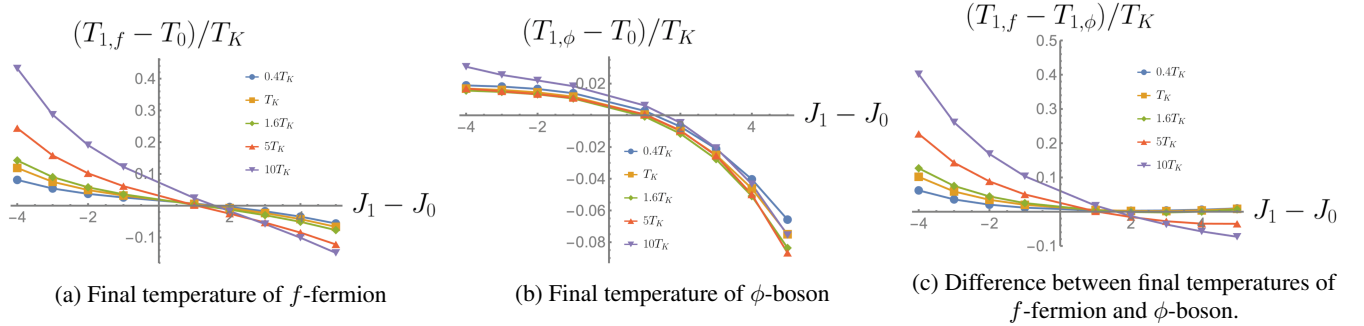


FIG. 7: Final temperatures after quenching as a function of $J_1 - J_0$ for the cases with the different initial temperatures given by $0.4T_K$, T_K , $1.6T_K$, $5T_K$, and $10T_K$.

For more quantitative analysis, we obtain the effective temperatures of the f -fermion and ϕ -boson using the Fluctuation-

Dissipation relations

$$\frac{iG_f^K(\mathcal{T}, \omega_r)}{A_f(\mathcal{T}, \omega_r)} = \tanh\left(\frac{\omega_r}{2T_f(\mathcal{T})}\right), \quad (49a)$$

$$\frac{iG_\phi^K(\mathcal{T}, \omega_r)}{A_\phi(\mathcal{T}, \omega_r)} = \coth\left(\frac{\omega_r}{2T_\phi(\mathcal{T})}\right) \quad (49b)$$

where $T_f(\mathcal{T})$ and $T_\phi(\mathcal{T})$ are the effective temperatures of the f -fermion and ϕ -boson respectively at the time \mathcal{T} . We found that the values of $T_f(\mathcal{T})$ and $T_\phi(\mathcal{T})$ converge as \mathcal{T} is increased. Let us set converged values of $T_f(\mathcal{T})$ and $T_\phi(\mathcal{T})$ to $T_{1,f}$ and $T_{1,\phi}$ respectively. Additionally, we also define the thermalization time as a difference between two times $\mathcal{T}_{0,f/\phi}$ and $\mathcal{T}_{1,f/\phi}$ where $\mathcal{T}_{0,f/\phi}$ is a time when the effective temperature $T_{f/\phi}(\mathcal{T})$ first deviates from the initial temperature T_0 in the forward time direction while $\mathcal{T}_{1,f/\phi}$ is a time when the effective temperature $T_{f/\phi}(\mathcal{T})$ first deviates from the final temperature $T_{1,f/\phi}$ in the backward time direction. As a qualitative criterion for the deviation, we used the following criteria: $\frac{|T_{f/\phi}(\mathcal{T}_{0/1,f/\phi}) - T_{0/1,f/\phi}|}{T_{0/1,f/\phi}} > 0.001$.

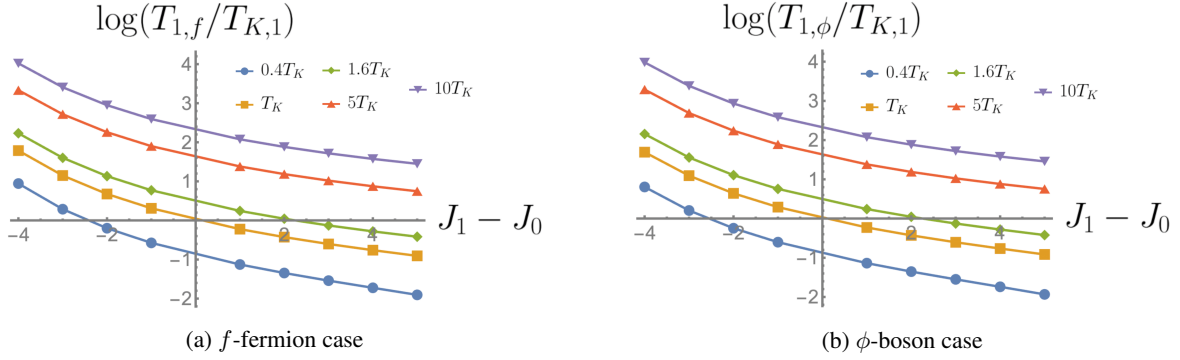


FIG. 8: Ratio between final temperatures and the Kondo temperatures ($T_{K,1} = \Lambda e^{-\frac{1}{J_1 N_F}}$) after quench as a function of $J_1 - J_0$ for the cases with the different initial temperatures given by $0.4T_K$, T_K , $1.6T_K$, $5T_K$ and $10T_K$.

Figure 7 shows the final temperatures of the f -fermion (Figure 7a), ϕ -boson (Figure 7b), and the temperature difference between them (Figure 7c). The figures clearly indicate that the f -fermion and ϕ -boson experience an increase in temperature as the coupling constant J_1 decreases below J_0 , whereas they experience a decrease in temperature when J_1 exceeds J_0 . This cooling effect arises due to the formation of the over-screened state, which occurs when the coupling between the impurity spin and the conduction electrons strengthens.

Furthermore, our observations reveal that the Kondo coupling constant J_1 must be greater than the initial value (J_0) for the system to attain thermal equilibrium, as evidenced by the equalization of the temperatures of the f -fermion and ϕ -boson shown in Figure 7c. Notably, when the initial state is the over-screened state, a Kondo coupling constant larger than the initial value is sufficient to ensure that the effective temperatures of the f -fermion and ϕ -boson are the same. In contrast to the over-screened state as the initial state, our observations suggest that achieving thermal equilibrium in a system with a high-temperature Fermi liquid state as the initial state requires a Kondo coupling constant larger than some threshold value. As the system approaches a non-Fermi liquid state, it becomes increasingly thermalized. To substantiate this proposition, we provide a phenomenological description employing the quantum Boltzmann equations in Section V.

When the Kondo coupling constant is decreased ($J_1 < J_0$), the f -fermion and the ϕ -boson thermalize into the states with the different temperatures shown in Fig. 7c. The physical reason for this temperature difference or partial-thermalization can be understood by the decoupling between the fermion and boson due to the higher final temperature compared to the Kondo temperature $T_{K,1}$ of the quenched system. Fig. 8 shows that the final temperatures of the partial thermalized cases are higher than the Kondo temperatures of the quenched system. As a result, f -fermion and ϕ -boson are decoupled and they are thermalized within their own Hilbert spaces separately with the different temperatures. The observed thermalization in the MCKI model is quite similar to the thermalization discussed in the mixed SYK model [53] containing both the SYK_2 and SYK_4 terms if we consider the partial-thermalized states in the MCKI model as pre-thermalized states specified with the slow thermalization in the SYK model. The analogy between the partial-thermalized states in the MCKI model and the pre-thermalized state in the SYK model becomes clear when we consider the re-feedback effect to the f -fermion and ϕ -boson from the conduction electron with the $1/N$ -correction. We will discuss it in the next section.

Now we discuss the thermalization time. Fig. 9 and 10 show the thermalization times of f -fermion and ϕ -boson for the cases with initial temperatures lower than the T_K and higher than the T_K respectively.

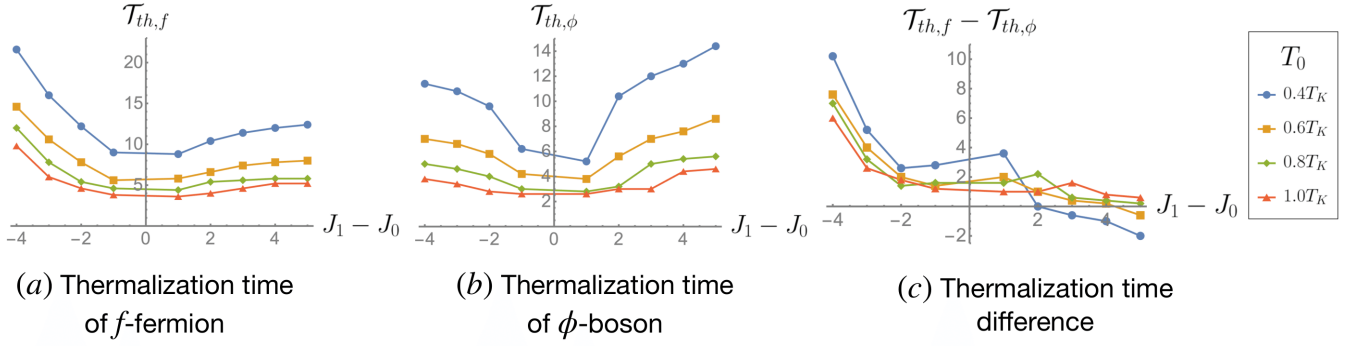


FIG. 9: Thermalization time as a function of $J_1 - J_0$ for thermalized cases with the initial temperatures given by $0.4T_K$, $0.6T_K$, $0.8T_K$, and $1.0T_K$.

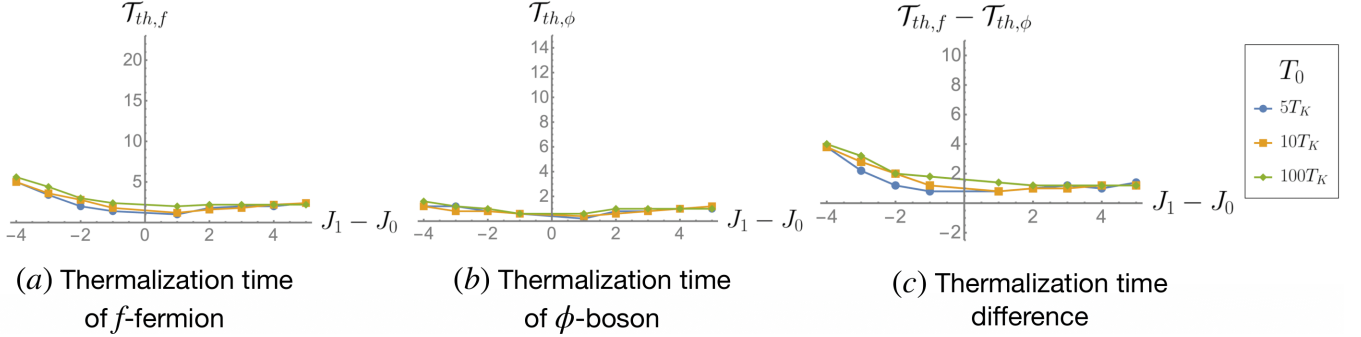


FIG. 10: Thermalization time as a function of $J_1 - J_0$ for thermalized cases with the initial temperatures given by $5T_K$, $10T_K$, and $100T_K$.

In case of the low initial temperatures ($\leq T_K$), both thermalization times $\mathcal{T}_{th,f}$ (Fig. 9 (a)) and $\mathcal{T}_{th,\phi}$ (Fig. 9 (b)) increase as the initial temperature is decreased. We expect that this is related to the non-Fermi liquid state formation in the low-temperature limit as discussed in [31]. The thermalization time difference in this case (Fig. 9 (c)) shows that there is a large thermalization time difference when $J_1 < J_0$ while not much difference when $J_1 > J_0$. This is consistent with the fact that the f -fermion and ϕ -boson are thermalized into the states with the same temperature when $T_0 \leq T_K$ and $J_1 > J_0$ while they are thermalized separately with different temperatures when $J_1 < J_0$.

Compared to the low initial temperature cases ($T_0 \leq T_K$), the thermalization times of high initial temperature cases ($T_0 \gg T_K$) do not depend on the initial temperature much as shown in Fig. 10. Additionally, their thermalization times are much shorter than that of the low initial temperature case. However, we should keep in mind that f -fermion and ϕ -boson in this case thermalize within their Hilbert spaces with different temperatures. To form a full thermalized state with the same temperature, it is necessary to consider the $1/N$ correction or re-feedback effect from the conduction electron. As a result, full thermalization time, in this case, might be much longer proportional to N .

2. Feedback effect to the conduction electron by the self-energy correction of order $\frac{1}{N}$



FIG. 11: One-loop self-energy correction of the order $\mathcal{O}(1/N)$ to the conduction electron.

In the large- N limit, there is no self-energy correction to the conduction electron. Therefore the temperature of the conduction electron remains at the initial temperature T_0 . Here by considering the feedback effect of the order $\frac{1}{N}$ from the f -fermion and ϕ -boson to the conduction electron, we argue the possibility of the full-thermalization by the re-feedback effect from the conduction

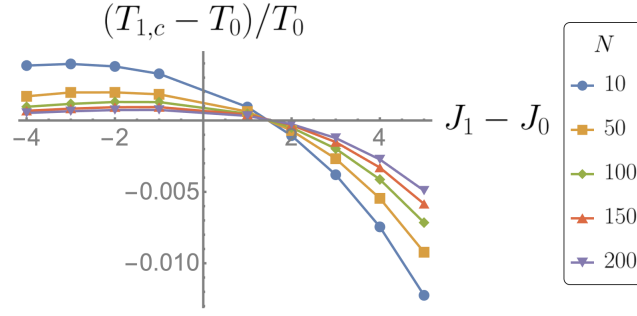


FIG. 12: Temperature difference of the conduction electron with the self-energy correction of $\mathcal{O}(N^{-1})$. Here $T_0 = 10T_K$ case is considered.

electron to the f -fermion and ϕ -boson.

To investigate the feedback effect to the conduction electron from f -fermion and ϕ -boson, we consider the one-loop self-energy correction, of order $1/N$ in Fig. 11, to the conduction electron and calculate the change of the conduction electron's effective temperature. For details of the Feynman rule, see Appendix. A. For simplicity, we calculate the $1/N$ self-energy correction in Fig. 11 using the solutions of Kadanoff-Baym equations (zeroth order in $1/N$) instead of solving the self-consistent equations including every $1/N$ -corrections. In the large- N limit, we expect that there would be not much difference between the solutions of the $1/N$ -correction obtained by the approximated way and exact way. For details of calculating the effective temperature with the $1/N$ -correction, see Appendix. D. Fig. 12 shows the change of the effective temperature of the conduction electron as a function of $J_1 - J_0$ for different N values. The larger the value of N , we can see that the temperature change decreases. With this feedback effect, the effective temperature of the conduction electron becomes closer to that of f -fermion and ϕ -boson. Therefore it is expected that this dressed conduction electron will give a re-feedback effect to the f -fermion and ϕ -boson and make them fully thermalize into the final state with the same temperature in a time scale proportional to the N . The fact that it takes a time scale proportional to N for the partial thermalized state to be the fully thermalized state makes the analogy we made between the partial thermalized states in the MCKI model and the pre-thermalized state in the SYK model more clear.

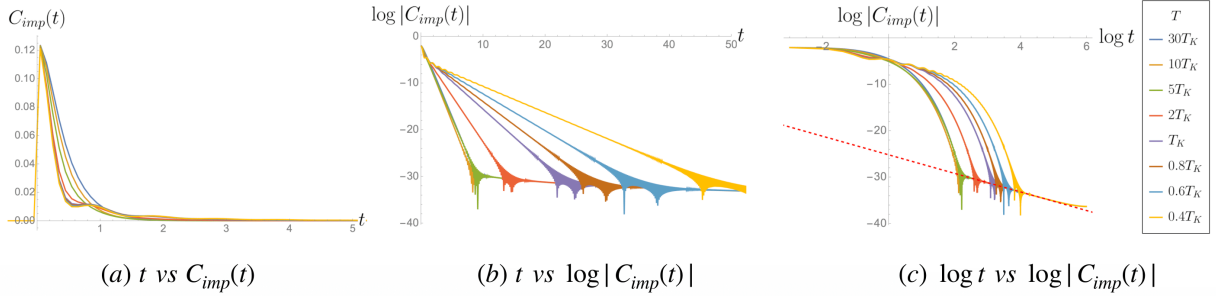


FIG. 13: $C_{imp}(t)$ of initial states with different temperatures ($30T_K$, $10T_K$, $5T_K$, $2T_K$, T_K , $0.8T_K$, $0.6T_K$ and $0.4T_K$). (a) t vs $C_{imp}(t)$ (b) t vs $\log |C_{imp}(t)|$ and (c) $\log t$ vs $\log |C_{imp}(t)|$. The slope of the fitting line (Red dashed line) in (c) is -2.

C. Spin-spin correlation function: $C_{imp}(\mathcal{T}, t_r)$ and $\chi_{imp}(\mathcal{T}, t_r)$.

In this section, we investigate the effects of the sudden quench on the impurity spin by considering the spin-spin correlation functions ($C_{imp}(\mathcal{T}, t_r)$ and $\chi_{imp}(\mathcal{T}, t_r)$). Before jumping into the non-equilibrium case, we first discuss the $C_{imp}(t)$ and $\chi_{imp}(t)$ in the equilibrium case.

Fig. 13 and Fig. 14 show the $C_{imp}(t)$ and $\chi_{imp}(t)$, their log plots and log-log plots respectively for different temperatures. From the log plots of $C_{imp}(t)$ (Fig. 13 (b)) and $\chi_{imp}(t)$ (Fig. 14 (b)), we can see that both $C_{imp}(t)$ and $\chi_{imp}(t)$ exponentially decay in the early time. Fig. 15 shows that the exponential decay rates of the $C_{imp}(t)$ and $\chi_{imp}(t)$ almost perfectly match each other. The exponential decay rate decreases rapidly as the temperature is reduced. In the long time limit, both $C_{imp}(t)$ and $\chi_{imp}(t)$ show the power-law decay as shown in Fig. 13 and 14 (c). However, they show the different power law exponents. For $C_{imp}(t)$, it is 2 while it is 3 for $\chi_{imp}(t)$. As a result, in the long time limit, $\langle \vec{S}_{imp}(t) \cdot \vec{S}_{imp}(0) \rangle$ shows the $\frac{1}{|t|^2}$ behavior which

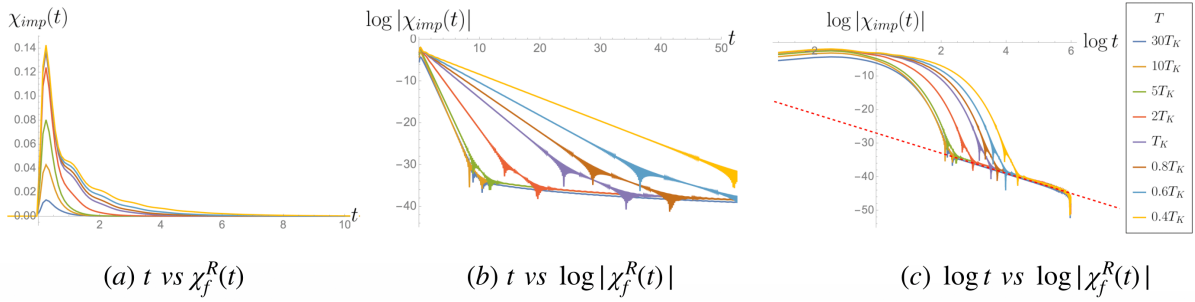


FIG. 14: $\chi_{imp}(t)$ of initial states with different temperatures ($30T_K$, $10T_K$, $5T_K$, $2T_K$, T_K , $0.8T_K$, $0.6T_K$ and $0.4T_K$). (a) t vs $\chi_{imp}(t)$ (b) t vs $\log |\chi_{imp}(t)|$ and (c) $\log t$ vs $\log |\chi_{imp}(t)|$. The slope of the fitting line (Red dashed line) in (c) is -3.

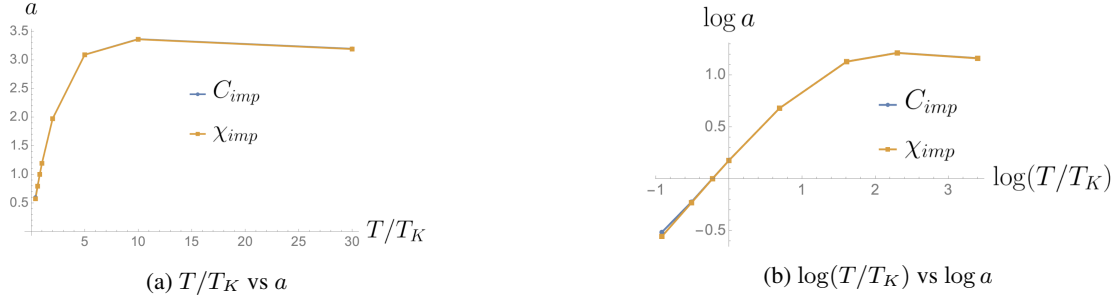


FIG. 15: Exponential decay rates of the C_{imp} and χ_{imp} ($C_{imp}(t), \chi_{imp}(t) \sim e^{-at}$) as a function of the temperature in equilibrium.

is consistent with the previous study done with the 2CK model [32].

Now let us turn our attention to the non-equilibrium case. Due to the limitation of the numerical power, it is more difficult to investigate the long time limit compared to the equilibrium case. Therefore we only focus on the transient dynamics of the $C_{imp}(\mathcal{T}, t_r)$ and $\chi_{imp}(\mathcal{T}, t_r)$. In the long time limit, we expect that the $C_{imp}(\mathcal{T}, t_r)$ and $\chi_{imp}(\mathcal{T}, t_r)$ show power law behaviors same to that observed in the equilibrium case [32].

Fig. 16 and 17 show the log plots of $C_{imp}(\mathcal{T}, t_r)$ and $\chi_{imp}(\mathcal{T}, t_r)$ with different values of \mathcal{T} all together to see the change of exponential decaying rates of them in transient time scale clearly.

When the $J_1 = 6$, the transient behaviours of $C_{imp}(\mathcal{T}, t_r)$ and $\chi_{imp}(\mathcal{T}, t_r)$ with $T_0 = 0.4T_K$ are quite similar to that of $T_0 = 10T_K$. The log plots for $J_1 = 6$ case in Fig. 16 and 17 show that the exponential decay rates of both the $C_{imp}(\mathcal{T}, t_r)$ and $\chi_{imp}(\mathcal{T}, t_r)$ decrease as \mathcal{T} increases. We expect that this is because the self-energy correction of f -fermion $\tilde{\Sigma}_f(t, t')$ (Eq. (30a)) is proportional to the J^2 which is supported by the fact that ratios between slopes of initial time (Dashed blue line in Fig. 16, 17) and later time (Dashed brown line in Fig. 16, 17) is close to the value $J_1^2/J_0^2 (= 0.36)$.

However when $J_1 = 15$, transient behaviours of $C_{imp}(\mathcal{T}, t_r)$ and $\chi_{imp}(\mathcal{T}, t_r)$ with $T_0 = 10T_K$ are quite different from that with $T_0 = 0.4T_K$. In the $T_0 = 10T_K$ case, the exponential decay rates are increased as \mathcal{T} is increased and values of increased rates are close to the value of $J_1^2/J_0^2 (= 2.25)$ as shown in Fig. 17. Therefore it can be understood with the previous argument based on the fact that self-energy $\tilde{\Sigma}_f(t, t')$ is proportional to J^2 . Unlike the $T_0 = 10T_K$ case, the exponential decay rates remain almost the same value in the $T_0 = 0.4T_K$ case (Fig. 17). It means that dissipation between the spin and conduction electron do not get stronger even the coupling between them increases.

Additionally, rapid oscillations after the quenching are observed in $C_{imp}(\mathcal{T}, t_r)$ and $\chi_{imp}(\mathcal{T}, t_r)$ only for the $T_0 = 0.4T_K$ case with $J_1 = 15$ as shown in Fig. 24, 25, 26, and 27 in Appendix. F.

These distinct features of the $T_0 = 0.4T_K$ case with $J_1 = 15$ can be understood because the impurity spin, in this case, is strongly entangled with conduction electrons, forming the over-screened Kondo state. Since this state is close to the eigenstate of the Kondo Hamiltonian, it does not react to the change of the Kondo coupling constant much. This is a contrasting feature compared to the $T_0 = 10T_K$ case where the state is closer to the eigenstate of the free fermion Hamiltonian. The oscillating pattern can be considered as one feature of the so-called revival in quench dynamics when the initial state is in a strongly entangled state [57]. Although the oscillating patterns are observed only when $T_0 = 0.4T_K$ with $J_1 = 15$ for $C_{imp}(\mathcal{T}, t_r)$ and $\chi_{imp}(\mathcal{T}, t_r)$, it turns out that these revivals happen regardless of values of J_1 as long as the initial state is given by the over-screened state in other physical quantities such as Kondo order parameter discussed in below.

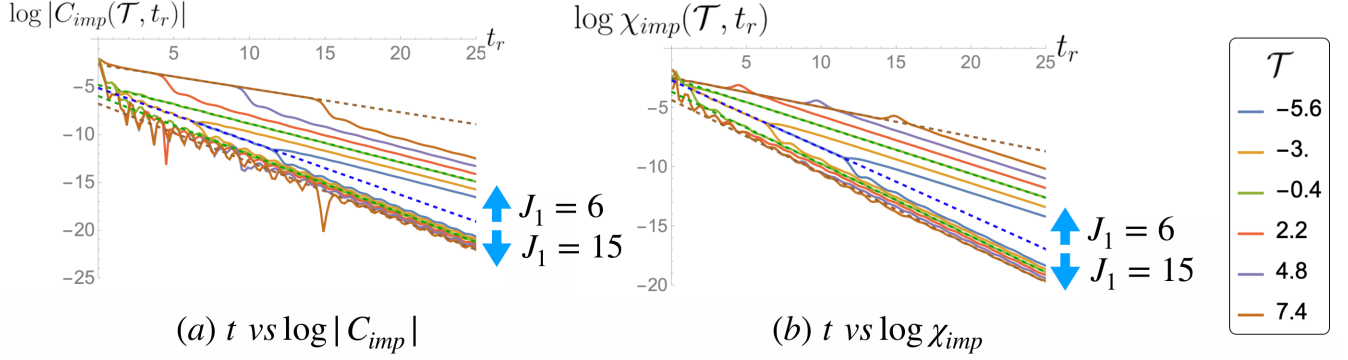


FIG. 16: Collection of the log plots of $\chi_{imp}(\mathcal{T}, t_r)$ and $C_{imp}(\mathcal{T}, t_r)$ for $T_0 = 0.4T_K$ case. The color of the graph denotes the values of \mathcal{T} . Dashed lines with blue, green and brown colors for both $J_1 = 6$ and $J_1 = 15$ cases are the linear fitting lines of the graphs at $\mathcal{T} = -5.6, -0.4$ and 7.4 respectively. Slopes of dashed lines in time order are given by $(-0.56, -0.4, -0.25)$ for C_{imp} with $J_1 = 6$, $(-0.56, -0.61, -0. - 0.61)$ for C_{imp} with $J_1 = 15$, $(-0.57, -0.4, -0.25)$ for χ_{imp} with $J_1 = 6$, and $(-0.57, -0.61, -0.61)$ for χ_{imp} with $J_1 = 15$.

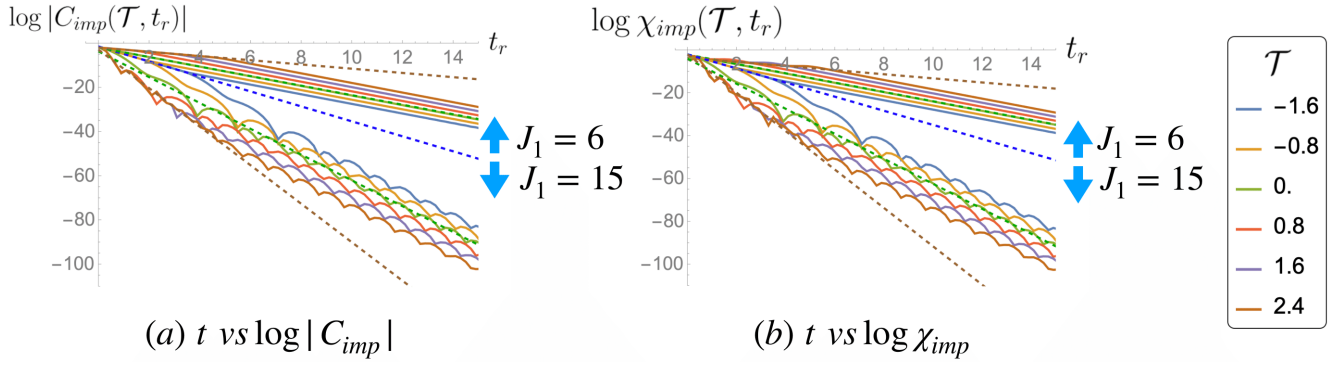


FIG. 17: Collection of the log plots of $\chi_{imp}(\mathcal{T}, t_r)$ and $C_{imp}(\mathcal{T}, t_r)$ for $T_0 = 10T_K$ case. The color of the graph denotes the values of \mathcal{T} . Dashed lines with blue, green and brown colors are the linear fitting lines of the graphs at $\mathcal{T} = -1.6, 0.0$ and 2.4 respectively. Slopes of dashed lines in time order are given by $(-3.4, -2.2, -1.0)$ for C_{imp} with $J_1 = 6$, $(-3.4, -5.8, -8.7)$ for C_{imp} with $J_1 = 15$, $(-3.3, -2.2, -1.0)$ for χ_{imp} with $J_1 = 6$, and $(-3.3, -5.81, -9.0)$ for χ_{imp} with $J_1 = 15$.

D. Kondo order parameter & Kondo energy density

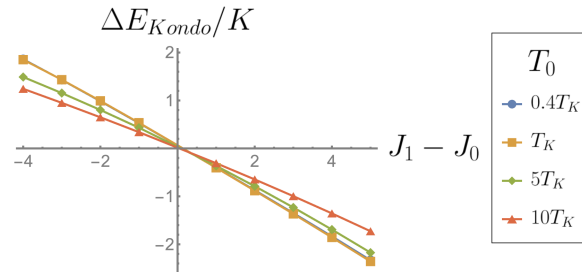


FIG. 18: Change of the Kondo energy before and after quench as a function of J_1 values for different initial temperatures. Here $\gamma = 0.8$.

In this section, we consider the evolution of the Kondo order parameter (Eq. (45)) and a change of the Kondo energy (Eq. (46)) after quench. Fig. 18 shows the change of the Kondo energy before and after the quench for different values of J_1 with different initial temperatures. As the temperature increases, the value of ΔE_{Kondo} decreases. This is because the states with higher temperatures have smaller absolute values of the Kondo energy. In other words, the impurity spin and the conduction electrons

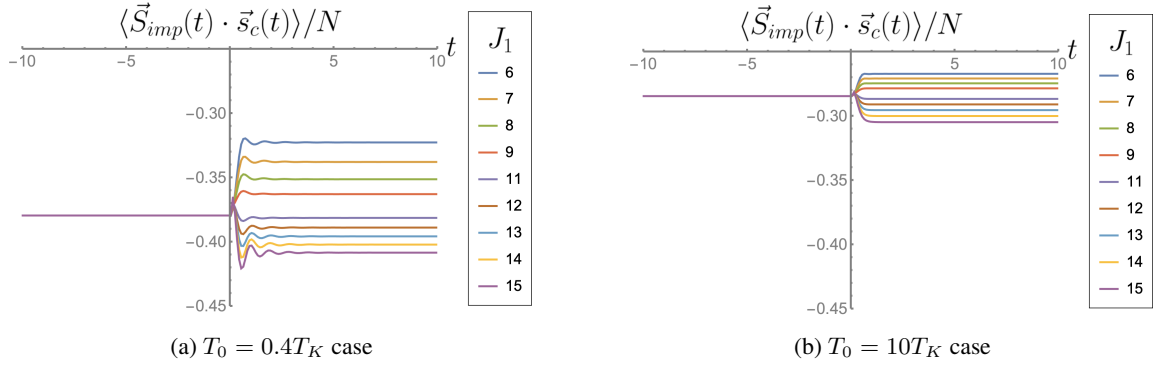


FIG. 19: Evolutions of the $\langle \vec{S}_{imp}(t) \cdot \vec{s}_c(t) \rangle / N$ for different J_1 values with $\gamma = 0.8$ and two different initial temperatures.

are almost decoupled for the high-temperature state.

A more interesting quantity to see is the evolution of the Kondo order parameter. Fig. 19 shows the evolution of the Kondo order parameter (Eq. (45)) for $T_0 = 0.4T_K$ and $T_0 = 10T_K$ respectively.

In both cases, the absolute values of the Kondo order parameter decrease when the coupling constant J is reduced while increasing when J increases. It is physically natural and expected results.

However, there is one major distinction between these two cases in the transient time scale. In the case of $T_0 = 10T_K$ (Fig. 19b), there are no oscillations in a transient time scale. In contrast to the $T_0 = 10T_K$ case, strong oscillating patterns are observed in the $T_0 = 0.4T_K$ case (Fig. 19a) for all J_1 values. Besides, it turns out that all frequencies of these oscillating patterns are the same regardless of the values of the J_1 and J_0 . More interestingly, the value of the frequency is given by Λ which is the energy cut-off of the conduction electron.

Since these oscillations are observed only when the initial state is closed to the over-screened Kondo state which is the strongly entangled state, it is expected that these oscillations are closely related to the revival phenomena in the quench dynamics of entangled states [57] as already discussed in Sec. IV C. Additionally, the universal frequency determined by only the cut-off of the conduction electron seems to be closely related to the observation of the universal frequency [56] in the spin-chain emulator of the two-impurity Kondo model and the frequency proportional to the Fermi velocity v_F in the free electron systems under the local quench [60–62].

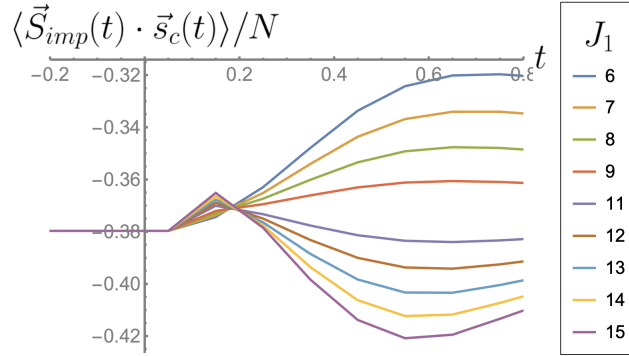


FIG. 20: Zoomed-in picture of the evolution of the Kondo order parameter in early time for $T_0 = 0.4T_K$ case.

As a final remark on the evolutions of the Kondo order parameter, we point out the sudden increment of the Kondo order parameter in the early time after the quench when J_1 is larger than the J_0 . Fig. 20 shows the zoomed-in picture of the evolution of the Kondo order parameter for the $T_0 = 0.4T_K$ case (Fig. 19a) in early time. As it is shown, the value of the Kondo order parameters suddenly increases in the early time when the J_1 is larger than the J_0 and decreases after that. This sudden increment of the Kondo order parameter for $J_1 > J_0$ cases can be understood easily by using the following identity for the Kondo order parameter:

$$\langle \vec{S}_{imp}(t) \cdot \vec{s}_c(t) \rangle = \left\langle \left[\left(\vec{S}_{imp}(t) + \vec{s}_c(t) \right)^2 - |\vec{S}_{imp}(t)|^2 - |\vec{s}_c(t)|^2 \right] \right\rangle \quad (50)$$

For simplicity, let us consider the $SU(2)$ case here. If we set $\vec{S}_{imp}(t) + \vec{s}_c(t) \equiv \vec{J}(t)$, then it is well known that the eigenstates

of $\vec{J}(t)$ are characterized by the quantum number j with degeneracy $2j + 1$. When an initial state is over-screened Kondo state in the low temperature, the first term of Eq. (50) should be very small to reduce the Kondo energy which means the value of j is small. Under the quench, the initial state with small j evolves to the states with larger j . Since the states with larger j have larger degeneracies, the value of the Kondo order parameter will become larger compared to the initial value. From this, we can understand why the value of the Kondo order parameter increases in the early time. If the initial state is in the high-temperature state, then the initial state is mainly characterized by the states with j of large values which have large degeneracy. In this case, there is much less chance for the initial state to evolve to the states with j of small value since they have smaller Hilbert space (smaller degeneracies). As a result, although there are also increments for the $T_0 = 10T_K$ case with J_1 larger than J_0 , the value is much smaller than that of the $T_0 = 0.4T_K$ case.

V. QUANTUM BOLTZMANN EQUATIONS

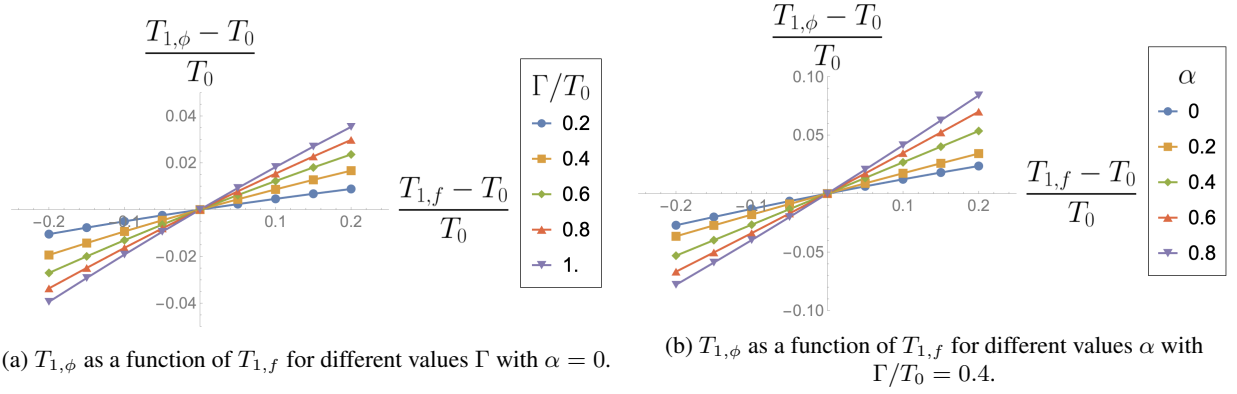


FIG. 21: $T_{1,\phi}$ as a function of $T_{1,f}$ with different values of Γ and α .

Following [54, 63], we derive the quantum Boltzmann equations. From Kadanoff-Baym equations (Eqs. (29)) and the parametrization of $G_{f,\phi}^K$ using the $F_{f,\phi}$ as follows

$$G_{f/\phi}^K = G_{f/\phi}^R \circ F_{f/\phi} - F_{f/\phi} \circ G_{f/\phi}^A, \quad (51)$$

we obtain the following quantum Boltzmann equations

$$\begin{aligned} \partial_{\mathcal{T}} F_f(\mathcal{T}, \omega_r) = & -\frac{\gamma J^2}{2} \int \frac{d\Omega}{2\pi} A_c(\omega_r + \Omega) A_\phi(\mathcal{T}, \Omega) \left[1 - F_c(\omega_r + \Omega) F_\phi(\mathcal{T}, \Omega) \right. \\ & \left. + \left(F_\phi(\mathcal{T}, \Omega) - F_c(\omega_r + \Omega) \right) F_f(\mathcal{T}, \omega_r) \right], \end{aligned} \quad (52a)$$

$$F_\phi(\mathcal{T}, \omega_r) = \frac{\int \frac{d\Omega}{2\pi} A_c(\omega_r + \Omega) A_f(\mathcal{T}, \Omega) [1 - F_c(\omega_r + \Omega) F_f(\mathcal{T}, \Omega)]}{\int \frac{d\Omega}{2\pi} A_c(\omega_r + \Omega) A_f(\mathcal{T}, \Omega) [F_c(\omega_r + \Omega) - F_f(\mathcal{T}, \Omega)]}. \quad (52b)$$

Here we use identities:

$$f = g \circ h : (\mathcal{T}, \omega_r) = g(\mathcal{T}, \omega_r) e^{\frac{i}{2} \left(\overleftarrow{\partial}_{\mathcal{T}} \overrightarrow{\partial}_{\omega_r} - \overleftarrow{\partial}_{\omega_r} \overrightarrow{\partial}_{\mathcal{T}} \right)} h(\mathcal{T}, \omega_r), \quad (53a)$$

$$f(t, t') = g(t, t') h(t', t) : f(\mathcal{T}, \omega_r) = \int \frac{d\omega_1}{2\pi} g(\mathcal{T}, \omega_r + \omega_1) h(\mathcal{T}, \omega_1). \quad (53b)$$

Here we ignore all derivative terms in Eq. (53a). We will justify this approximation in the below.

Note that $F_\phi(\mathcal{T}, \omega_r)$ is determined only by $A_f(\mathcal{T}, \Omega)$ and $F_f(\mathcal{T}, \Omega)$ from Eq. (53b). Although the above quantum Boltzmann equations are much simpler than Kadanoff-Baym equations, it is still quite difficult to obtain the analytical solutions. Therefore instead of solving the full quantum Boltzmann equations, we use only Eq. (53b) to discuss how the final temperature of ϕ -boson depends on a form of the spectral function and the final temperature of the f -fermion phenomenologically. Since we assume the final state a long time after the quench, the assumption of ignoring all derivative terms can be justified.

Let us assume the temperature of the final state of f -fermion is given by $T_{1,f}$ then $F_f(\omega) = \tanh\left(\frac{\omega}{2T_{1,f}}\right)$. Additionally using the fact that $F_c(\omega) = \tanh\left(\frac{\omega}{2T_0}\right)$, $A_c(\omega) \propto \theta(\Lambda - |\omega|)$ where T_0 is the temperature of the conduction bath, Eq. (53b) is simplified into

$$F_\phi(\omega_r) = \frac{\int_{-\Lambda}^{\Lambda} \frac{d\Omega}{2\pi} A_f(\Omega - \omega_r) \coth\left(\frac{\Omega}{2T_0} - \frac{\Omega - \omega_r}{2T_{1,f}}\right) \left[\tanh\left(\frac{\Omega}{2T_0}\right) - \tanh\left(\frac{\Omega - \omega_r}{2T_{1,f}}\right) \right]}{\int_{-\Lambda}^{\Lambda} \frac{d\Omega}{2\pi} A_f(\Omega - \omega_r) \left[\tanh\left(\frac{\Omega}{2T_0}\right) - \tanh\left(\frac{\Omega - \omega_r}{2T_{1,f}}\right) \right]} \quad (54)$$

where we have used the identity: $\tanh(x - y) = \frac{\tanh x - \tanh y}{1 - \tanh x \tanh y}$.

As a general form of $A_f(\Omega)$, we set

$$A_f(\Omega) = 2 \frac{\Gamma + |\Omega|^{1-\alpha} \sin\left(\frac{\alpha\pi}{2}\right)}{|\Omega|^{2(1-\alpha)} \cos^2\left(\frac{\alpha\pi}{2}\right) + \left(\Gamma + |\Omega|^{1-\alpha} \sin\left(\frac{\alpha\pi}{2}\right)\right)^2}, \quad (0 \leq \alpha < 1) \quad (55)$$

where Γ is a constant scattering rate and α is an anomalous dimension originating from the Kondo interaction. The above spectral function is obtained from the Matsubara Green's function of the form $G_f(i\omega_n) = \frac{1}{i\omega_n |\omega_n|^{-\alpha} + i \text{sgn}(\omega_n) \Gamma}$ by analytic continuation.

$A_f(\Omega)$ with $\alpha = 0$ is a usual spectral function of the Fermi liquid state with the scattering rate Γ while $A_f(\Omega)$ with the non-zero α describes non-Fermi liquid state. In the Multi-Channel Kondo system, the high-temperature state of f -fermion can be considered as a Fermi liquid state with the finite scattering rate due to the conduction electron while the low-temperature state is a non-Fermi liquid state so-called over-screened state with α is given by $\frac{1}{1+\gamma}$ [14].

As a phenomenological approach to understanding the difference of final effective temperatures of f -fermion ($T_{1,f}$) and ϕ -boson ($T_{1,\phi}$) for different quench protocols, we obtain the final effective temperature of ϕ -boson for a given value of $T_{1,f}$ with different forms of $A_f(\Omega)$ by varying α and Γ .

If we consider the $T_{1,f} = T_0$ case as a sanity check, one can easily check that the $F_\phi(\omega_r) = \coth\left(\frac{\omega_r}{2T_0}\right)$ from Eq. (54) regardless of the form of $A_f(\Omega)$. It is consistent with the fact that the system is in the equilibrium state.

Now let us consider when $T_{1,f}$ is different from T_0 . By fitting the numerically obtained $F_\phi(\omega_r)$ with $\coth\left(\frac{\omega_r}{2T_{1,\phi}}\right)$, we obtain values of $T_{1,\phi}$. Fig. 21 shows the values of $(T_{1,\phi} - T_0)/T_0$ as a function of $(T_{1,f} - T_0)/T_0$ for different Γ values with $\alpha = 0$ (Fig. 21 (a)) and different α values with the fixed Γ (Fig. 21 (b)).

From Fig. 21, we can clearly see that the final temperature of ϕ -boson becomes closer to that of f -fermion as the scattering rate Γ and the anomalous dimension α increase. To some extent, it explains why the temperature difference between the f -fermion and the ϕ -boson becomes smaller when we consider the quench with the larger J values and the initial temperature lower than T_K where the initial state is given by the non-Fermi liquid state. Additionally, the analysis here shows that the magnitude of difference between the $T_{1,\phi}$ and T_0 ($= (T_{1,\phi} - T_0)/T_0$) is always smaller than that between $T_{1,f}$ and T_0 ($= (T_{1,f} - T_0)/T_0$) as shown in Fig. 21. It is consistent with the numerical results discussed in Sec. IV B 1.

VI. CONCLUSION

In this paper, we have investigated the thermalization and transient behavior in the Multi-Channel Kondo system under the sudden quantum quench of the Kondo coupling constant using the SU(N) MCKI model and Keldysh formalism with the large- N method. From the numerical analysis and phenomenological analysis using quantum Boltzmann equations, we found that the system is equilibrated (i.e., the final temperatures of the f -fermion and ϕ -boson are given by the same value) when the final state is the over-screened state which is specified by the final temperature lower than the Kondo temperature of the post-quench Kondo coupling constant J_1 . Otherwise, the system evolves to the state specified with two different effective temperatures of f -fermion and ϕ -boson. The non-equilibrated state with different effective temperatures of f and ϕ indicates that the feedback effect to the conduction electrons by the $1/N$ correction of the self-energy needs to be considered for the system to be equilibrated, and it is shown that the dressed conduction electrons would be able to eventually thermalize the full system with the thermalization time proportional to N . In addition to the thermalization phenomena, we discuss the quantum cooling effect observed when the Kondo coupling constant is increased in relation to the reduction of the impurity entropy.

Regarding the transient non-equilibrium properties, we discuss the evolutions of the spin-spin correlation functions, the Kondo order parameter, and the Kondo energy density. From the evolutions of the spin-spin correlation function with several different conditions, we found that the exponential decay rate does not change when the initial state is given by the over-screened state and the Kondo coupling constant is increased. Otherwise, the exponential decay rates change during the transient time and they are

proportional to the square of the Kondo coupling constants. In addition, we found general oscillation patterns with the universal frequency given by the cut-off of the conduction electron in every physical quantity during the transient time scale for the initial state being the over-screened state. Otherwise, there are no such oscillations observed during the transient time. The oscillation patterns observed only for the over-screened initial state are closely related to the revival generally observed in the entangled state under the quench [57]. Moreover, the universal frequency is given by the cut-off of the conduction electrons expected to be related to the entanglement spreading by the conduction electron in the local quantum quenched system [60–62].

Through our study, the non-equilibrium properties of the MCKI model under the sudden quantum quench are systematically analyzed. We provide complementary results to the previous studies [31–37] mostly focusing on the steady states. Also considering its large- N structure, we expect that our results can give guidance in studying the non-equilibrium phenomena in the MCKI model using CFT [14] and holographic methods [38]. Additionally using the same framework, it is possible to study more general non-equilibrium set-ups for different physical systems. One interesting physical system to be considered is the pseudo gap Kondo Impurity model [64–66]. Since it is well known that the pseudo-gap Kondo system hosts a quantum phase transition [66], it would be interesting to study transient non-equilibrium phenomena such as the dynamical quantum phase transition (DQPT) [67] in this system. Another interesting direction is to investigate the transient non-equilibrium current through the multi-channel Kondo impurity under the sudden quenching of lead voltages. This quench protocol mainly discussed using heavy numerical methods such as quantum Monte Carlo (QMC) [68–71], density matrix renormalization group (DMRG) [72–75], and time-dependent numerical renormalization group (TDNRG) [29, 76, 77] methods. We expect that our findings provide new insights into the non-equilibrium dynamics of the MCKI model in the transient time scale and motivate further exploration of transient non-equilibrium phenomena in the MCKI model.

ACKNOWLEDGEMENTS

I.J acknowledge the discussion with Franchesco Piazza. We thank Stefan Kirchner and Chung-Hou Chung for the discussion and the National Center for Theoretical Sciences (NCTS) for the support. This work is supported by the National Science and Technology Council of Taiwan under Grants No. NSTC 112- 2636-M-007-007.

Appendix A: Derivation of the large- N saddle point self-consistent equations using the Feynman diagrams

Here we provide a derivation of the saddle point self-consistent equations (Eq. (14)) using Feynman diagrams. Based on the Hubbard-Stratonovich transformed action Eq. (9), we obtain following Feynman rules:

$$z \longrightarrow z' = -i\langle f_\alpha(z')f_\beta^\dagger(z) \rangle = \delta_{\alpha\beta}G_f(z', z) \quad (\text{A1a})$$

$$z \dashrightarrow z' = -i\langle c_{i\alpha}(z')c_{j\beta}^\dagger(z) \rangle = \delta_{ij}\delta_{\alpha\beta}G_c(z', z) \quad (\text{A1b})$$

$$z \rightsquigarrow z' = -i\langle B_i(z')B_j^\dagger(z) \rangle = \delta_{ij}G_B(z', z) \quad (\text{A1c})$$

$$i, \alpha \dashrightarrow \begin{array}{c} \alpha \\ \nearrow \\ \text{---} \\ \searrow \\ i \end{array} = -\frac{i}{\sqrt{N}}, \quad i, \alpha \dashleftarrow \begin{array}{c} \alpha \\ \nwarrow \\ \text{---} \\ \swarrow \\ i \end{array} = -\frac{i}{\sqrt{N}} \quad (\text{A1d})$$

Using the above Feynman rules, one-loop self energies of the f fermion and the B boson are given by

$$\Sigma_f(z', z) = \begin{array}{c} \frac{1}{\sqrt{N}} \dashrightarrow \\ \text{---} \\ \frac{1}{\sqrt{N}} \dashrightarrow \end{array} = i\gamma G_c(z', z)G_B(z, z'), \quad (\text{A2})$$

$$\Sigma_B(z', z) = \begin{array}{c} \frac{1}{\sqrt{N}} \dashrightarrow \\ \text{---} \\ \frac{1}{\sqrt{N}} \dashrightarrow \end{array} = iG_c(z', z)G_f(z, z') \quad (\text{A3})$$

where

$$G_f^{-1} = G_{f,0}^{-1} - \Sigma_f, \quad G_B^{-1} = -J^{-1} + \Sigma_B. \quad (\text{A4})$$

It can be easily checked that the self-energies of the f and B with more than one loop and the self-energy of the conduction electron c are suppressed by the $\frac{1}{N}$ factor. As a result, Eqs. (A2) and (A3) become exact in the $N \rightarrow \infty$ limit.

Using the above Feynman rules, one-loop self energies of the f fermion and the B boson are given by

Appendix B: Preparation of the Initial state

1. Kadanoff-Baym equation in the equilibrium

Consider an initial state with a Kondo coupling J_0 at temperature T_0 . Since the initial state is assumed to be in equilibrium, we change all bi-local fields $\mathcal{O}(t, t')$ into $\mathcal{O}(t - t')$. Then the resulting self-consistent equations of the Green's functions; $G_{f/c/\phi}^{>/</R}(t)$ from the Kadanoff-Baym equations (29) are given as follows:

$$G_f^R(\omega) = \frac{1}{\omega \pm i\eta - \lambda_0 + i\gamma J G_c^<(t=0) - \tilde{\Sigma}_f^R(\omega)}, \quad (\text{B1a})$$

$$G_\phi^R(\omega) = \frac{\Sigma_B^R(\omega)}{J \Sigma_B^R(\omega) - 1} \quad (\text{B1b})$$

where

$$\tilde{\Sigma}_f^{>/<}(t) = i\gamma J^2 G_\phi^{</>}(-t) G_c^{>/<}(t), \quad (\text{B2a})$$

$$\Sigma_B^{>/<}(t) = i G_f^{</>}(-t) G_c^{>/<}(t), \quad (\text{B2b})$$

$$G_f^<(t=0) = iq_0, G_f^>(t=0) = -i(1 - q_0) \quad (\text{B2c})$$

and

$$G_f^R(t) = \Theta(t)[G_f^>(t) - G_f^<(t)], \quad (\text{B3a})$$

$$\tilde{\Sigma}_f^R(t) = \Theta(t)[\tilde{\Sigma}_f^>(t) - \tilde{\Sigma}_f^<(t)], \quad (\text{B3b})$$

$$G_\phi^R(t) = \Theta(t)[G_\phi^>(t) - G_\phi^<(t)]. \quad (\text{B3c})$$

2. Kubo-Martin-Schwinger (KMS) condition

To take account of the initial temperature T_0 , KMS condition needs to be considered. For the Green's function G_f , G_c and G_ϕ , the following KMS conditions are used:

$$G_{f/c}^<(\omega) = -e^{-\beta\omega} G_{f/c}^>(\omega) \Rightarrow \begin{cases} G_{f/c}^>(\omega) = -i(1 - n_F(\omega))A_{f/c}(\omega) \\ G_{f/c}^<(\omega) = in_F(\omega)A_{f/c}(\omega) \end{cases}, \quad (\text{B4})$$

$$G_\phi^<(\omega) = e^{-\beta\omega} G_\phi^>(\omega) \Rightarrow \begin{cases} G_\phi^>(\omega) = -i(1 + n_B(\omega))A_\phi(\omega) \\ G_\phi^<(\omega) = -in_B(\omega)A_\phi(\omega) \end{cases} \quad (\text{B5})$$

where $A_{f/c/\phi} = -2ImG_{f/c/\phi}^R$ and $n_{F/B}(\omega) = \frac{1}{e^{\beta\omega} \pm 1}$.

3. Analytic form of the Green's functions of the conduction electrons

Since there is no self-energy correction to the conduction electron, it is a just non-interacting trivial case. Therefore we can obtain an analytic form of the $A_c(\omega)$ and $G_c^{>/<}(\omega)$ using the Eq. (10a) and the KMS condition Eq. (B4) as follows:

$$A_c(\omega) = -2ImG_c^R(\omega) \approx \frac{2\pi V D_F}{N_{site}} \int_{-\Lambda}^{\Lambda} d\epsilon \delta(\omega - \epsilon) = \frac{2\pi V D_F}{N_{site}} \Theta(\Lambda - |\omega|) \quad (\text{B6})$$

$$\begin{cases} G_c^>(\omega) = -i\left(1 - n_F(\omega)\right)2\pi \frac{V D_F}{N_{site}} \Theta(\Lambda - |\omega|), \\ G_c^<(\omega) = in_F(\omega)2\pi \frac{V D_F}{N_{site}} \Theta(\Lambda - |\omega|) \end{cases} \quad (\text{B7})$$

where V and D_F are the volume of the system and a density of states near the Fermi energy per volume respectively and Λ is an energy cut-off near the Fermi energy point. Self-consistency of the above results can be easily shown. Here we consider only conduction electrons near the Fermi energy based on the physical assumption that only conduction electrons near Fermi energy will play an important role.

If we do not make the approximation that only conduction electrons near Fermi energy are considered then an integration of the $A_c(\omega)$ to ω is given by value 1 as follows:

$$\int \frac{d\omega}{2\pi} A_c(\omega) = \frac{1}{N_{site}} \sum_p = 1 \quad (B8)$$

However due to the approximation, the sum-rule of $A_c(\omega)$ is changed and the integration of the $A_c(\omega)$ with respect to ω should be smaller than the value 1. Therefore

$$\int \frac{d\omega}{2\pi} A_c(\omega) = \frac{VD_F}{N_{site}} \int d\omega \Theta(\Lambda - |\omega|) = \frac{2\Lambda VD_F}{N_{site}} < 1 \quad (B9)$$

Here $2\Lambda VD_F$ is a number of conduction electrons within the energy regime $-\Lambda < \epsilon < \Lambda$ near the Fermi energy. We will use a notation $\nu_c = \frac{2\Lambda VD_F}{N_{site}}$ as a conduction electron filling in the remaining context. Then,

$$A_c(\omega) = \frac{\nu_c \pi}{\Lambda} \Theta(\Lambda - |\omega|), \quad (B10)$$

$$G_c^>(\omega) = -i(1 - n_F(\omega)) \frac{\nu_c \pi}{\Lambda} \Theta(\Lambda - |\omega|), \quad G_c^<(\omega) = i n_F(\omega) \frac{\nu_c \pi}{\Lambda} \Theta(\Lambda - |\omega|). \quad (B11)$$

For the density of states of the conduction electron near the Fermi energy, we use the notation N_f which is given by $\frac{\nu_c}{2\Lambda}$ in terms of ν_c and Λ .

4. Flow chart of programming

The numerical process to obtain the initial states is given as follows:

1. Prepare initial guess: $G_f^{>/<, (0)}(t)$, $G_\phi^{>/<, (0)}(t)$
 \Downarrow
2. Calculate the self energies: $\tilde{\Sigma}_f^{>/<, (0)}(t)$, $\Sigma_B^{>/<, (0)}(t) \rightarrow \tilde{\Sigma}_f^{R, (0)}(t)$, $\Sigma_B^{R, (0)}(t)$
 \Downarrow
3. Find λ_0 value satisfying the condition: $G_f^<(t=0) = i q_0$, $G_f^>(t=0) = -i(1 - q_0)$
 \Downarrow
4. Define new retarded Green's function (updating an effect of interaction):

$$G_f^{R, (0)} = x G_{f,1}^R [G_f^{>/<, (0)}] + (1-x) G_{f,2}^R [\tilde{\Sigma}_f^{R, (0)}, \lambda],$$

$$G_\phi^{R, (0)} = x G_{\phi,1}^R [G_\phi^{>/<, (0)}] + (1-x) G_{\phi,2}^R [\Sigma_\phi^{R, (0)}]$$
 \Downarrow
5. Obtain new greater and lesser Green's function using KMS conditions:

$$G_f^{>, (1)}(\omega) = -i(1 - n_F(\omega)) A_f [G_f^{R, (0)}], \quad G_f^{<, (1)}(\omega) = i n_F(\omega) A_f [G_f^{R, (0)}]$$

$$G_\phi^{>, (1)}(\omega) = -i(1 + n_B(\omega)) A_\phi [G_\phi^{R, (0)}], \quad G_\phi^{<, (1)}(\omega) = -i n_B(\omega) A_\phi [G_\phi^{R, (0)}]$$
 \Downarrow
6. Go to step 2 and continue the same step until following convergence conditions hold:

$$|G_{f/\phi}^{>/<, (n+1)} - G_{f/\phi}^{>/<, (n)}| / |G_{f/\phi}^{>/<, (n)}| \ll \epsilon$$

where

$$\begin{aligned}
G_{f/\phi,1}^R \left[G_{f/\phi}^{>/<,(n)} \right] &= \Theta(t) [G_{f/\phi}^{>,(n)} - G_{f/\phi}^{<,(n)}], \\
G_{f,2}^R \left[\tilde{\Sigma}_f^{R,(n)}, \lambda \right] &= \frac{1}{\omega + i\eta - \lambda + i\gamma J G_c^<(t=0) - \tilde{\Sigma}_f^{R,(n)}(\omega)}, \\
G_{\phi,2}^R \left[\Sigma_\phi^{R,(n)} \right] &= \frac{\Sigma_\phi^{R,(n)}(\omega)}{J \Sigma_\phi^{R,(n)}(\omega) - 1}.
\end{aligned}$$

Appendix C: Numerical Details of solving the Kadanoff-Baym equations

Here we give details of numerical simulation of Kadanoff-Baym equations (Eq. (29)).

1. Discrete forms of Kadanoff-Baym equations

To solve the Kadanoff-Baym equations numerically, we need to express the continuous Kadanoff-Baym equations into discrete form first. Using the fact that the differentiation and the integration can be expressed in the discrete forms as follows: $\partial_t f(t) = \frac{f(t+\Delta t) - f(t)}{\Delta t}$ and $\int_{-\infty}^{\infty} dt f(t) = \sum_{-T/2 \leq t \leq T/2} f(t) \Delta t$ where T is the total time length, we get following discrete Kadanoff-Baym equations from Eq. (29):

$$\begin{aligned}
& i \frac{G_f^{R/A}(t + \Delta t, t') - G_f^{R/A}(t, t')}{\Delta t} + \left(-\lambda_0 + i\gamma J(t) G_c^<(t, t) \right) G_f^{R/A}(t, t') \\
& - \Delta t \sum_{-T/2 \leq \bar{t} \leq T/2} \tilde{\Sigma}_f^{R/A}(t, \bar{t}) G_f^{R/A}(\bar{t}, t') = \frac{\delta_{t,t'}}{\Delta t}, \tag{C1a}
\end{aligned}$$

$$\begin{aligned}
& i \frac{G_f^{>/<}(t + \Delta t, t') - G_f^{>/<}(t, t')}{\Delta t} + \left(-\lambda_0 + i\gamma J(t) G_c^<(t, t) \right) G_f^{>/<}(t, t') \\
& = \Delta t \left[\sum_{-T/2 \leq \bar{t} \leq t'} \tilde{\Sigma}_f^{>/<}(t, \bar{t}) G_f^A(\bar{t}, t') + \sum_{-T/2 \leq \bar{t} \leq t} \tilde{\Sigma}_f^R(t, \bar{t}) G_f^{>/<}(\bar{t}, t') \right], \tag{C1b}
\end{aligned}$$

$$G_\phi^{R/A}(t, t') + \Sigma_B^{R/A}(t, t') = \Delta t \sum_{-T/2 \leq \bar{t} \leq T/2} \Sigma_B^{R/A}(t, \bar{t}) J(\bar{t}) G_\phi^{R/A}(t, t'), \tag{C1c}$$

$$\begin{aligned}
& G_\phi^{>/<}(t, t') + \Sigma_B^{>/<}(t, t') = \Delta t \left[\sum_{-T/2 \leq \bar{t} \leq t'} \Sigma_B^{>/<}(t, \bar{t}) J(\bar{t}) G_\phi^A(\bar{t}, t') \right. \\
& \left. + \sum_{-T/2 \leq \bar{t} \leq t} \Sigma_B^R(t, \bar{t}) J(\bar{t}) G_\phi^{>/<}(\bar{t}, t') \right] \tag{C1d}
\end{aligned}$$

where

$$G^R(t, t') = \Theta(t - t') (G^>(t, t') - G^<(t, t')), \quad \Theta(t - t') = \begin{cases} 1 & t > t' \\ 1/2 & t = t' \\ 0 & t < t' \end{cases}, \quad (\text{C2a})$$

$$\tilde{\Sigma}_f^{>/<}(t, t') = i\gamma J(t)J(t')G_\phi^{</>}(t', t)G_c^{>/<}(t, t'), \quad (\text{C2b})$$

$$\Sigma_B^{>/<}(t, t') = iG_f^{</>}(t', t)G_c^{>/<}(t, t'), \quad (\text{C2c})$$

$$G_f^{<}(t, t) = iq_0, \quad G_f^{>}(t, t) = -i(1 - q_0), \quad G_f^{R/A}(t, t) = \mp \frac{i}{2}, \quad (\text{C2d})$$

$$G_\phi^{R/A}(t, t) = \mp i \frac{q_0 \nu_c + iG_c^{<}(t, t)}{2} \quad (\text{Eq. (34)}), \quad (\text{C2e})$$

$$[G_{c/f/\phi}^{>/<}(t, t')]^* = -G_{c/f/\phi}^{>/<}(t', t), \quad [G_{c/f/\phi}^R(t, t')]^* = G_{c/f,\phi}^A(t', t), \quad (\text{C2f})$$

$$[\Sigma_{c/B}^{>/<}(t, t')]^* = -\Sigma_{c/B}^{>/<}(t', t), \quad [\Sigma_{c/B}^R(t, t')]^* = \Sigma_{c/B}^A(t', t), \quad (\text{C2g})$$

$$[\tilde{\Sigma}_f^{>/<}(t, t')]^* = -\tilde{\Sigma}_f^{>/<}(t', t), \quad [\tilde{\Sigma}_f^R(t, t')]^* = \tilde{\Sigma}_f^A(t', t) \quad (\text{C2h})$$

2. Flow chart of solving the discrete KB equations

Fig. 22 shows the flow chart of Kadanoff-Baym equations solver. For simplicity, only the predictor step is shown in the flow chart. In the actual simulation, we use the Adams-Bashforth-Moulton method [78] which is Predictor-Corrector type scheme to reduce the numerical error.

(i) From the initial states and the sum-rules (Eq. (C2d) and (C2e)),

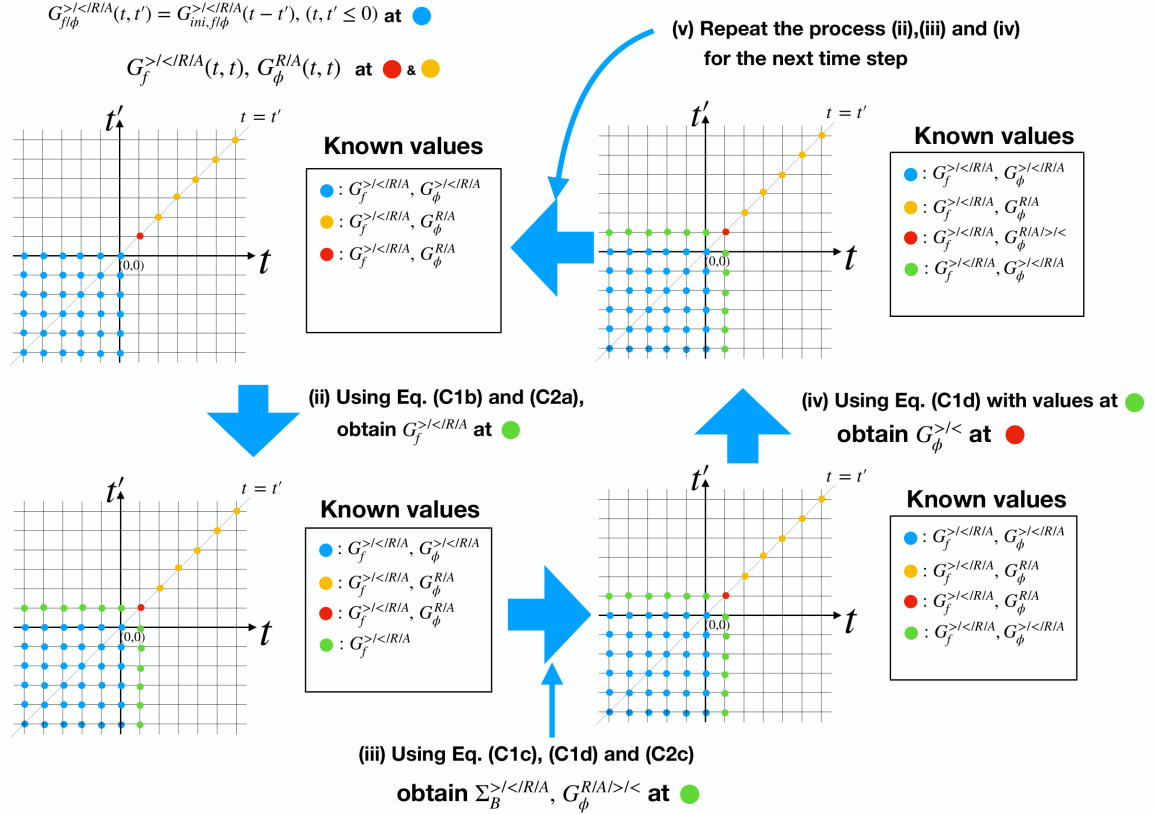


FIG. 22: Flow chart of the Kadanoff-Baym equation solver

Appendix D: Effective temperature of the conduction electron with $1/N$ -self energy correction

The Keldysh-Schwinger equation for the conduction electrons with the one-loop self energy correction of order $1/N$ given in Fig. 11 is given by

$$\int_c d\bar{z} [G_c^{-1}(z, \bar{z}) - \Sigma_c(z, \bar{z})] \bar{G}_c(z, z') = \delta(z - z'), \quad (\text{D1a})$$

$$\Sigma_c(z, z') = \frac{i}{N} G_f(z, z') G_B(z, z') \quad (\text{D1b})$$

where $G_c^{-1}(z, z') = G_{c,0}^{-1}(z, z') + \frac{q_0}{N} J(z) \delta(z - z')$ and $\bar{G}_c(z, z')$ is a one-loop self energy included Green's function of conduction electron.

Using Eq. (25) and $G_f^<(t, t) = iq_0$, the above equations become

$$\int_c d\bar{z} [G_{c,0}^{-1}(z, \bar{z}) - \tilde{\Sigma}_c(z, \bar{z})] \bar{G}_c(z, z') = \delta(z - z'), \quad (\text{D2a})$$

$$\tilde{\Sigma}_c(z, z') = \frac{i}{N} J(z) J(z') G_f(z, z') G_\phi(z, z'). \quad (\text{D2b})$$

Applying the Keldysh rotation, we can obtain the following Kadanoff-Baym equations of conduction electrons consisting of retarded, advanced, and Keldysh Green's function with real-time arguments:

$$[G_{c,0}^{-1} - \tilde{\Sigma}_c] \circ \bar{G}_c = \mathbf{1} \quad (\text{D3})$$

where \circ notation means the matrix product in the Keldysh and time space. Here $G_{c,0}^{-1}$, $\tilde{\Sigma}_c$ and \bar{G}_c are matrices given by

$$G_{c,0}^{-1} = \begin{pmatrix} (G_{c,0}^R)^{-1} & -(G_{c,0}^R)^{-1} G_{c,0}^K (G_{c,0}^A)^{-1} \\ 0 & (G_{c,0}^A)^{-1} \end{pmatrix},$$

$$\tilde{\Sigma}_c = \begin{pmatrix} \tilde{\Sigma}_c^R & \tilde{\Sigma}_c^K \\ 0 & \tilde{\Sigma}_c^A \end{pmatrix}, \quad \bar{G}_c = \begin{pmatrix} \bar{G}_c^R & \bar{G}_c^K \\ 0 & \bar{G}_c^A \end{pmatrix}$$

Using the above matrix expressions and Eq. (D3), we obtain the $\bar{G}_c^{R/A}$ and \bar{G}_c^K in terms of the $G_{c,0}^{R/A/K}$ and $\tilde{\Sigma}_c^{R/A/K}$ as follows:

$$\bar{G}_c^{R/A} = [(G_{c,0}^{R/A})^{-1} - \tilde{\Sigma}_c^{R/A}]^{-1}, \quad (\text{D4})$$

$$\begin{aligned} \bar{G}_c^K &= [(G_{c,0}^R)^{-1} - \tilde{\Sigma}_c^R]^{-1} \circ \left([G_{c,0}^R]^{-1} G_{c,0}^K [G_{c,0}^A]^{-1} + \tilde{\Sigma}_c^K \right) \circ [G_{c,0}^A]^{-1} - \tilde{\Sigma}_c^A]^{-1} \\ &= \bar{G}_c^R \circ \left([G_{c,0}^R]^{-1} G_{c,0}^K [G_{c,0}^A]^{-1} + \tilde{\Sigma}_c^K \right) \circ \bar{G}_c^A \end{aligned} \quad (\text{D5})$$

Using the Fluctuation-Dissipation relation: $\lim_{T \rightarrow \infty} \frac{i\bar{G}_c^K(T, \omega_r)}{-2Im\bar{G}_c^R(T, \omega_r)} \approx \tanh\left(\frac{\omega_r}{2T_{1,c}}\right)$, the effective temperatures of the conduction electron shown in Fig. 12 can be obtained.

Appendix E: Sanity check: sum-rules

In Sec. III C 1 of the main text, the sum rules are discussed. Here the numerical results of the sum-rules using Eqs. (32) and (34) are presented as sanity checks. For simplicity, we provide the only sum rules of $J_1 = 6$ and $J_1 = 15$ cases with the initial temperature $T_0 = 0.4T_K$ here.

Fig. 23 shows the numerical results of the sum-rules: Eqs. (32) and (34). Although the numerical values shown in Fig. 23 should be zero in principle, it shows deviations from the zero value due to the numerical errors. Increasing the number of the time lattices and reducing the time step Δt reduce these errors. However, these deviations are so small that they do not affect to results much.

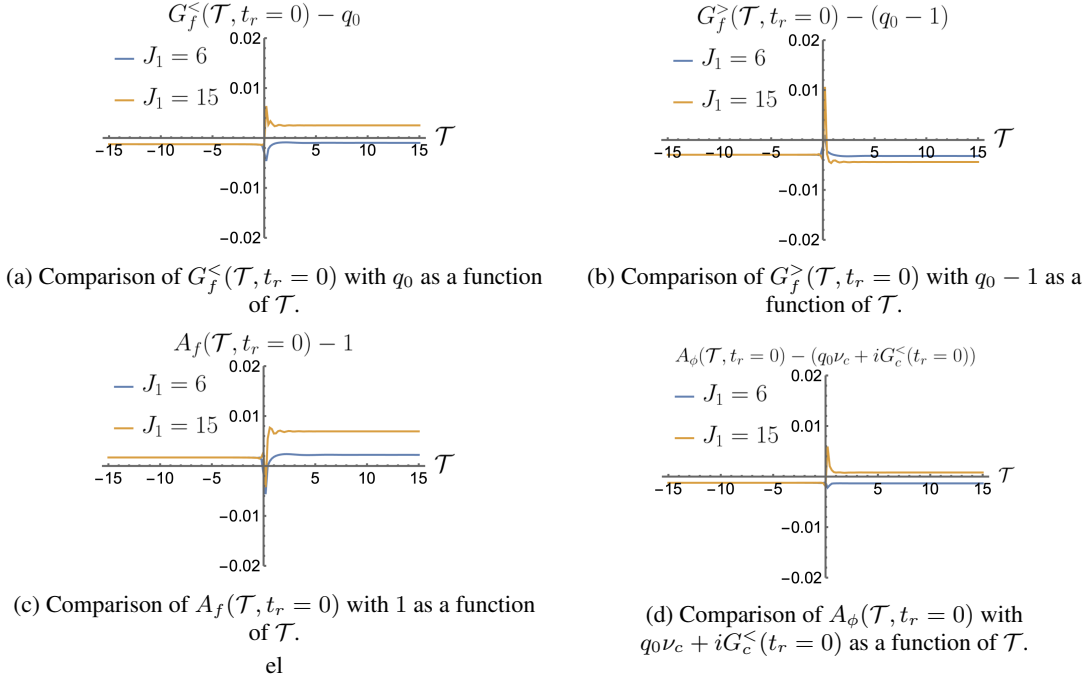


FIG. 23: Sum-rules of $J_1 = 6$ and $J_1 = 15$ cases with the initial temperature $T_0 = 0.4T_K$ and $J_0 = 10$. Numerical values of the q_0 and ν_c are given by 0.5 in this numerical simulation. Blue and yellow lines denote the cases with $J_1 = 6$ and $J_1 = 15$ respectively.

Appendix F: Evolutions of $\mathcal{C}_{imp}(\mathcal{T}, t_r)$ and $\chi_{imp}(\mathcal{T}, t_r)$ after the quenching for $T_0 = 10T_K$ and $T_0 = 0.4T_K$ cases with $J_1 = 6, 15$.

Here we present the numerical solutions of $\mathcal{C}_{imp}(\mathcal{T}, t_r)$ and $\chi_{imp}(\mathcal{T}, t_r)$ for $T_0 = 10T_K$ and $T_0 = 0.4T_K$ cases with $J_1 = 6, 15$.

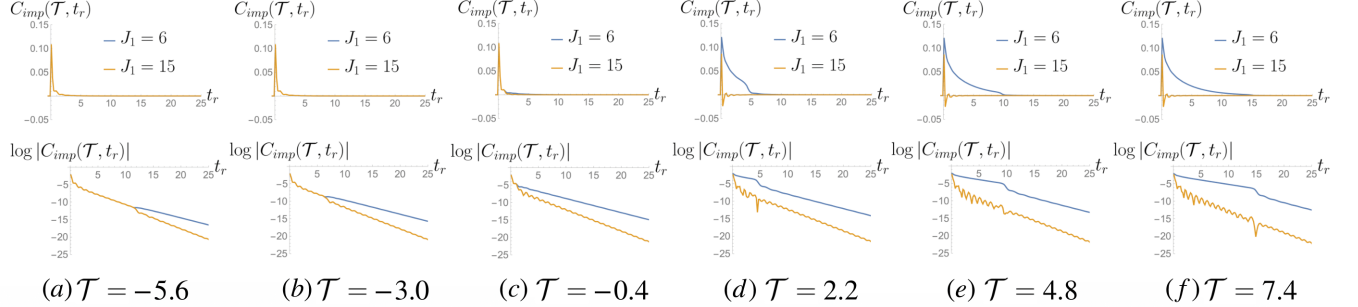


FIG. 24: Evolution of $\mathcal{C}_{imp}(\mathcal{T}, t_r)$ for $T_0 = 0.4T_K$ case with J_1 is given by 6 and 15. The figures of first and second row correspond to t_r vs $\mathcal{C}_{imp}(\mathcal{T}, t_r)$ and t_r vs $\ln |\mathcal{C}_{imp}(\mathcal{T}, t_r)|$ respectively.

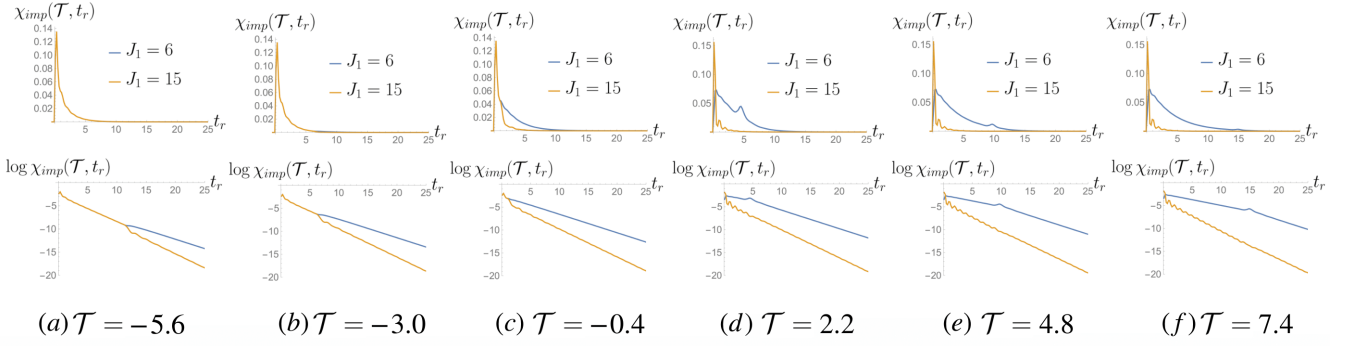


FIG. 25: Evolution of the Spin susceptibility $\chi_{imp}(\mathcal{T}, t_r)$ for $T_0 = 0.4T_K$ case with J_1 is given by 6 and 15. The figures of first and second row correspond to t_r vs $\chi_{imp}(\mathcal{T}, t_r)$ and t_r vs $\ln \chi_{imp}(\mathcal{T}, t_r)$ respectively.

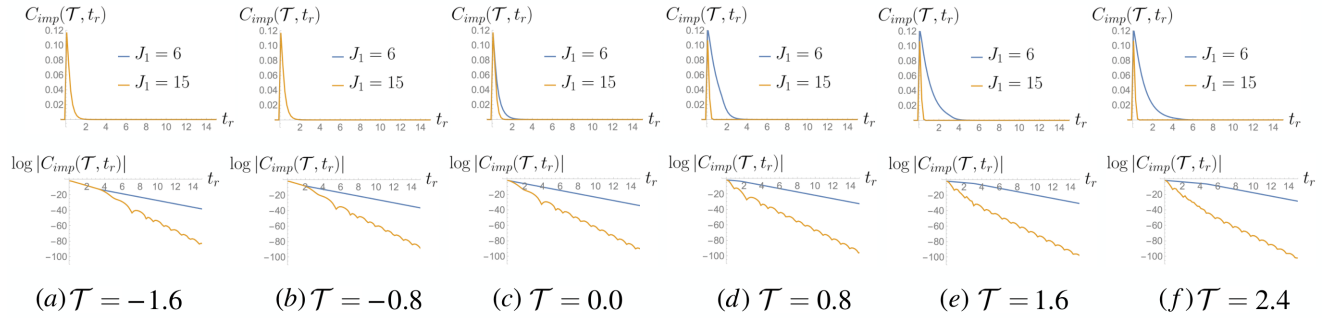


FIG. 26: Evolution of $C_{imp}(\mathcal{T}, t_r)$ for $T_0 = 10T_K$ case with J_1 is given by 6 and 15. The figures of first and second row correspond to t_r vs $C_{imp}(\mathcal{T}, t_r)$ and t_r vs $\ln C_{imp}(\mathcal{T}, t_r)$ respectively.

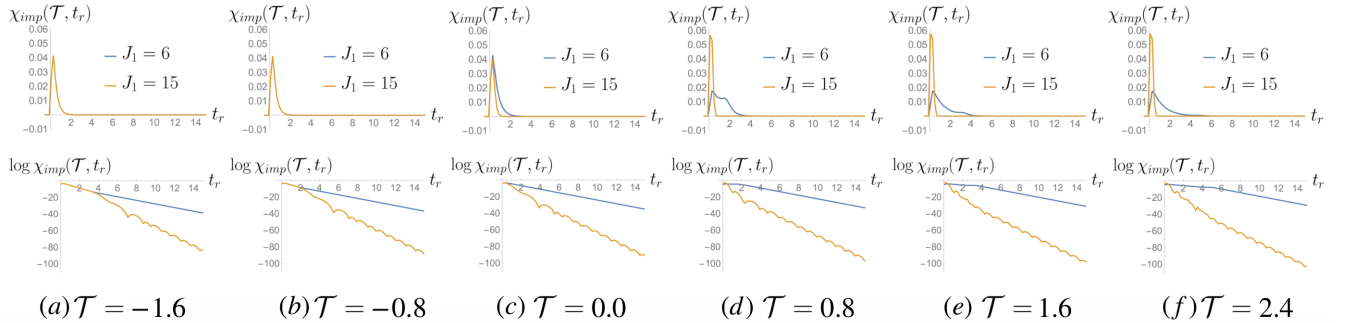


FIG. 27: Evolution of the Spin susceptibility $\chi_{imp}(\mathcal{T}, t_r)$ for $T_0 = 10T_K$ case with J_1 is given by 6 and 15. The figures of first and second row correspond to t_r vs $\chi_{imp}(\mathcal{T}, t_r)$ and t_r vs $\ln \chi_{imp}(\mathcal{T}, t_r)$ respectively

-
- [1] P. Schlottmann and P. Sacramento, Multichannel kondo problem and some applications, *Advances in Physics* **42**, 641 (1993), <https://doi.org/10.1080/00018739300101534>.
- [2] J. Kondo, Resistance Minimum in Dilute Magnetic Alloys, *Progress of Theoretical Physics* **32**, 37 (1964), <https://academic.oup.com/ptp/article-pdf/32/1/37/5193092/32-1-37.pdf>.
- [3] C. L. Seaman, M. B. Maple, B. W. Lee, S. Ghamaty, M. S. Torikachvili, J.-S. Kang, L. Z. Liu, J. W. Allen, and D. L. Cox, Evidence for non-fermi liquid behavior in the kondo alloy $y_{1-x}u_x\text{pd}_3$, *Phys. Rev. Lett.* **67**, 2882 (1991).
- [4] B. Andraka and A. M. Tsvelik, Observation of non-fermi-liquid behavior in $u_{0.2}y_{0.8}\text{pd}_3$, *Phys. Rev. Lett.* **67**, 2886 (1991).
- [5] D. C. Ralph and R. A. Buhrman, Observations of kondo scattering without magnetic impurities: A point contact study of two-level tunneling systems in metals, *Phys. Rev. Lett.* **69**, 2118 (1992).
- [6] V. J. Emery and S. Kivelson, Mapping of the two-channel kondo problem to a resonant-level model, *Phys. Rev. B* **46**, 10812 (1992).

- [7] I. Affleck and A. W. W. Ludwig, Critical theory of overscreened Kondo fixed points, *Nucl. Phys. B* **360**, 641 (1991).
- [8] A. W. W. Ludwig and I. Affleck, Exact conformal field theory results on the multichannel Kondo effect: Asymptotic three-dimensional space and time dependent multipoint and many particle Green's functions, *Nucl. Phys. B* **428**, 545 (1994).
- [9] I. Affleck, A Current Algebra Approach to the Kondo Effect, *Nucl. Phys. B* **336**, 517 (1990).
- [10] J. Gan, N. Andrei, and P. Coleman, Perturbative approach to the non-fermi-liquid fixed point of the overscreened kondo problem, *Phys. Rev. Lett.* **70**, 686 (1993).
- [11] N. Andrei and C. Destri, Solution of the multichannel kondo problem, *Phys. Rev. Lett.* **52**, 364 (1984).
- [12] N. Andrei and A. Jerez, Fermi- and non-fermi-liquid behavior in the anisotropic multichannel kondo model: Bethe ansatz solution, *Phys. Rev. Lett.* **74**, 4507 (1995).
- [13] R. Bulla, T. A. Costi, and T. Pruschke, Numerical renormalization group method for quantum impurity systems, *Rev. Mod. Phys.* **80**, 395 (2008).
- [14] O. Parcollet, A. Georges, G. Kotliar, and A. Sengupta, Overscreened multichannel $SU(n)$ kondo model: Large- n solution and conformal field theory, *Phys. Rev. B* **58**, 3794 (1998).
- [15] L. A. Landau, E. Cornfeld, and E. Sela, Charge fractionalization in the two-channel kondo effect, *Phys. Rev. Lett.* **120**, 186801 (2018).
- [16] D. Gabay, C. Han, P. L. S. Lopes, I. Affleck, and E. Sela, Multi-impurity chiral kondo model: Correlation functions and anyon fusion rules, *Phys. Rev. B* **105**, 035151 (2022).
- [17] M. Papaj, Z. Zhu, and L. Fu, Multichannel charge kondo effect and non-fermi-liquid fixed points in conventional and topological superconductor islands, *Phys. Rev. B* **99**, 014512 (2019).
- [18] J. von Delft, D. Ralph, R. Buhrman, S. Upadhyay, R. Louie, A. Ludwig, and V. Ambegaokar, The 2-channel kondo model: I. review of experimental evidence for its realization in metal nanoconstrictions, *Annals of Physics* **263**, 1.
- [19] J. von Delft, A. Ludwig, and V. Ambegaokar, The 2-channel kondo model: II. cft calculation of non-equilibrium conductance through a nanoconstriction containing 2-channel kondo impurities, *Annals of Physics* **273**, 175 (1999).
- [20] S. Kirchner, Two-channel kondo physics: From engineered structures to quantum materials realizations, *Advanced Quantum Technologies* **3**, 1900128 (2020), <https://onlinelibrary.wiley.com/doi/pdf/10.1002/qute.201900128>.
- [21] R. M. Potok, I. G. Rau, H. Shtrikman, Y. Oreg, and D. Goldhaber-Gordon, Observation of the two-channel kondo effect, *Nature* **446**, 167 (2007).
- [22] L. Zhu, G. Woltersdorf, and J. Zhao, Observation of orbital two-channel kondo effect in a ferromagnetic 110-mnnga film, *Scientific Reports* **6**, 34549 (2016).
- [23] S. Gupta, R. Sachan, and J. Narayan, Emergence of orbital two-channel kondo effect in epitaxial tin thin films, *Solid State Communications* **341**, 114547 (2022).
- [24] B. Dóra, M. A. Werner, and C. u. u. u. P. m. c. Moca, Information scrambling at an impurity quantum critical point, *Phys. Rev. B* **96**, 155116 (2017).
- [25] X. Han and Z. Yu, Quantum chaos of the bose-fermi kondo model at intermediate temperature, *Phys. Rev. B* **104**, 085139 (2021).
- [26] M. Lotem, E. Sela, and M. Goldstein, Manipulating non-abelian anyons in a chiral multichannel kondo model, *Phys. Rev. Lett.* **129**, 227703 (2022).
- [27] M. Pletyukhov and H. Schoeller, Nonequilibrium kondo model: Crossover from weak to strong coupling, *Phys. Rev. Lett.* **108**, 260601 (2012).
- [28] F. B. Anders and A. Schiller, Real-time dynamics in quantum-impurity systems: A time-dependent numerical renormalization-group approach, *Phys. Rev. Lett.* **95**, 196801 (2005).
- [29] F. B. Anders and A. Schiller, Spin precession and real-time dynamics in the kondo model: Time-dependent numerical renormalization-group study, *Phys. Rev. B* **74**, 245113 (2006).
- [30] C.-Y. Lin, Y.-Y. Chang, C. Rylands, N. Andrei, and C.-H. Chung, Universal nonequilibrium $i - v$ curve near the two-channel kondo-luttinger quantum critical point, *Phys. Rev. B* **102**, 075145 (2020).
- [31] Z. Ratiani and A. Mitra, Nonequilibrium dynamics of a two-channel kondo system due to a quantum quench, *Phys. Rev. B* **81**, 125110 (2010).
- [32] M. Heyl and S. Kehrein, Interaction quench dynamics in the kondo model in the presence of a local magnetic field, *Journal of Physics: Condensed Matter* **22**, 345604 (2010).
- [33] G. A. R. van Dalum, A. K. Mitchell, and L. Fritz, Electric and heat transport in a charge two-channel kondo device, *Phys. Rev. B* **102**, 205137 (2020).
- [34] G. A. R. van Dalum, A. K. Mitchell, and L. Fritz, Wiedemann-franz law in a non-fermi liquid and majorana central charge: Thermoelectric transport in a two-channel kondo system, *Phys. Rev. B* **102**, 041111 (2020).
- [35] D. B. Karki and M. N. Kiselev, Quantum thermoelectric and heat transport in the overscreened kondo regime: Exact conformal field theory results, *Phys. Rev. B* **102**, 241402 (2020).
- [36] S. Kirchner and Q. Si, Quantum criticality out of equilibrium: Steady state in a magnetic single-electron transistor, *Phys. Rev. Lett.* **103**, 206401 (2009).
- [37] P. Ribeiro, Q. Si, and S. Kirchner, Local quantum criticality out of equilibrium: Effective temperatures and scaling in the steady-state regime, *Europhysics Letters* **102**, 50001 (2013).
- [38] J. Erdmenger, M. Flory, M.-N. Newrzella, M. Strydom, and J. M. S. Wu, Quantum quenches in a holographic kondo model, *Journal of High Energy Physics* **2017**, 45 (2017).
- [39] A. Eberlein, V. Kasper, S. Sachdev, and J. Steinberg, Quantum quench of the sachdev-ye-kitaev model, *Phys. Rev. B* **96**, 205123 (2017).
- [40] Y. Gu, A. Lucas, and X.-L. Qi, Spread of entanglement in a sachdev-ye-kitaev chain, *Journal of High Energy Physics* **2017**, 120 (2017).
- [41] R. Bhattacharya, D. P. Jatkar, and N. Sorokhaibam, Quantum quenches and thermalization in syk models, *Journal of High Energy Physics* **2019**, 66 (2019).

- [42] M. Haque and P. A. McClarty, Eigenstate thermalization scaling in majorana clusters: From chaotic to integrable sachdev-ye-kitaev models, *Phys. Rev. B* **100**, 115122 (2019).
- [43] A. Haldar, P. Haldar, S. Bera, I. Mandal, and S. Banerjee, Quench, thermalization, and residual entropy across a non-fermi liquid to fermi liquid transition, *Phys. Rev. Res.* **2**, 013307 (2020).
- [44] P. Zhang, Entanglement entropy and its quench dynamics for pure states of the sachdev-ye-kitaev model, *Journal of High Energy Physics* **2020**, 143 (2020).
- [45] C. Kuhlenskamp and M. Knap, Periodically driven sachdev-ye-kitaev models, *Phys. Rev. Lett.* **124**, 106401 (2020).
- [46] T. Samui and N. Sorokhaibam, Thermalization in different phases of charged syk model, *Journal of High Energy Physics* **2021**, 157 (2021).
- [47] Y. Cheipesh, A. I. Pavlov, V. Ohanesjan, K. Schalm, and N. V. Gnedilov, Quantum tunneling dynamics in a complex-valued sachdev-ye-kitaev model quench-coupled to a cool bath, *Phys. Rev. B* **104**, 115134 (2021).
- [48] C. Liu, P. Zhang, and X. Chen, Non-unitary dynamics of Sachdev-Ye-Kitaev chain, *SciPost Phys.* **10**, 048 (2021).
- [49] A. Kulkarni, T. Numasawa, and S. Ryu, Lindbladian dynamics of the sachdev-ye-kitaev model, *Phys. Rev. B* **106**, 075138 (2022).
- [50] C. Zanoci and B. Swingle, Energy transport in sachdev-ye-kitaev networks coupled to thermal baths, *Phys. Rev. Res.* **4**, 023001 (2022).
- [51] C. Zanoci and B. Swingle, Near-equilibrium approach to transport in complex sachdev-ye-kitaev models, *Phys. Rev. B* **105**, 235131 (2022).
- [52] R. Sohal, L. Nie, X.-Q. Sun, and E. Fradkin, Thermalization of randomly coupled syk models, *Journal of Statistical Mechanics: Theory and Experiment* **2022**, 013103 (2022).
- [53] A. Larzul and M. Schiró, Quenches and (pre)thermalization in a mixed sachdev-ye-kitaev model, *Phys. Rev. B* **105**, 045105 (2022).
- [54] A. Larzul, S. J. Thomson, and M. Schiro, Are fast scramblers good thermal baths? (2022), [arXiv:2204.06434](https://arxiv.org/abs/2204.06434).
- [55] P. O. Boykin, T. Mor, V. Roychowdhury, F. Vatan, and R. Vrijen, Algorithmic cooling and scalable nmr quantum computers, *Proceedings of the National Academy of Sciences* **99**, 3388 (2002), <https://www.pnas.org/doi/pdf/10.1073/pnas.241641898>.
- [56] A. Bayat, S. Bose, H. Johannesson, and P. Sodano, Universal single-frequency oscillations in a quantum impurity system after a local quench, *Phys. Rev. B* **92**, 155141 (2015).
- [57] A. A. Michailidis, C. J. Turner, Z. Papić, D. A. Abanin, and M. Serbyn, Slow quantum thermalization and many-body revivals from mixed phase space, *Phys. Rev. X* **10**, 011055 (2020).
- [58] H. Aoki, N. Tsuji, M. Eckstein, M. Kollar, T. Oka, and P. Werner, Nonequilibrium dynamical mean-field theory and its applications, *Rev. Mod. Phys.* **86**, 779 (2014).
- [59] P. Coleman, *Introduction to Many-Body Physics* (Cambridge University Press, 2015).
- [60] P. Calabrese and J. Cardy, Entanglement and correlation functions following a local quench: a conformal field theory approach, *Journal of Statistical Mechanics: Theory and Experiment* **2007**, P10004 (2007).
- [61] V. Eisler and I. Peschel, Evolution of entanglement after a local quench, *Journal of Statistical Mechanics: Theory and Experiment* **2007**, P06005 (2007).
- [62] J.-M. Stéphan and J. Dubail, Local quantum quenches in critical one-dimensional systems: entanglement, the loschmidt echo, and light-cone effects, *Journal of Statistical Mechanics: Theory and Experiment* **2011**, P08019 (2011).
- [63] A. Kamenev, *Field Theory of Non-Equilibrium Systems* (Cambridge University Press, 2011).
- [64] D. Withoff and E. Fradkin, Phase transitions in gapless fermi systems with magnetic impurities, *Phys. Rev. Lett.* **64**, 1835 (1990).
- [65] K. Chen and C. Jayaprakash, The kondo effect in pseudo-gap fermi systems: a renormalization group study, *Journal of Physics: Condensed Matter* **7**, L491 (1995).
- [66] L. Fritz and M. Vojta, Phase transitions in the pseudogap anderson and kondo models: Critical dimensions, renormalization group, and local-moment criticality, *Phys. Rev. B* **70**, 214427 (2004).
- [67] M. Heyl, Dynamical quantum phase transitions: a review, *Reports on Progress in Physics* **81**, 054001 (2018).
- [68] P. Werner, T. Oka, M. Eckstein, and A. J. Millis, Weak-coupling quantum monte carlo calculations on the keldysh contour: Theory and application to the current-voltage characteristics of the anderson model, *Phys. Rev. B* **81**, 035108 (2010).
- [69] M. Schiró, Real-time dynamics in quantum impurity models with diagrammatic monte carlo, *Phys. Rev. B* **81**, 085126 (2010).
- [70] A. E. Antipov, Q. Dong, and E. Gull, Voltage quench dynamics of a kondo system, *Phys. Rev. Lett.* **116**, 036801 (2016).
- [71] I. Krivenko, J. Kleinhenz, G. Cohen, and E. Gull, Dynamics of kondo voltage splitting after a quantum quench, *Phys. Rev. B* **100**, 201104 (2019).
- [72] M. A. Cazalilla and J. B. Marston, Time-dependent density-matrix renormalization group: A systematic method for the study of quantum many-body out-of-equilibrium systems, *Phys. Rev. Lett.* **88**, 256403 (2002).
- [73] S. Kirino, T. Fujii, J. Zhao, and K. Ueda, Time-dependent dmrg study on quantum dot under a finite bias voltage, *Journal of the Physical Society of Japan* **77**, 084704 (2008), <https://doi.org/10.1143/JPSJ.77.084704>.
- [74] F. Heidrich-Meisner, A. E. Feiguin, and E. Dagotto, Real-time simulations of nonequilibrium transport in the single-impurity anderson model, *Phys. Rev. B* **79**, 235336 (2009).
- [75] S. Kirino and K. Ueda, Nonlinear transport through quantum dots studied by the time-dependent dmrg, *Annalen der Physik* **523**, 664 (2011), <https://onlinelibrary.wiley.com/doi/pdf/10.1002/andp.201100031>.
- [76] E. Eidelstein, A. Schiller, F. Güttge, and F. B. Anders, Coherent control of correlated nanodevices: A hybrid time-dependent numerical renormalization-group approach to periodic switching, *Phys. Rev. B* **85**, 075118 (2012).
- [77] H. T. M. Nghiem and T. A. Costi, Time evolution of the kondo resonance in response to a quench, *Phys. Rev. Lett.* **119**, 156601 (2017).
- [78] W. H. Press, S. A. Teukolsky, W. T. Vetterling, and B. P. Flannery, *Numerical Recipes 3rd Edition: The Art of Scientific Computing*, 3rd ed. (Cambridge University Press, 2007).